



This is a repository copy of *Identification and characterisation of hypomethylated DNA loci controlling quantitative resistance in Arabidopsis*.

White Rose Research Online URL for this paper:
<http://eprints.whiterose.ac.uk/140662/>

Version: Accepted Version

Article:

Furci, L., Jain, R., Stassen, J. orcid.org/0000-0001-5483-325X et al. (7 more authors)
(2019) Identification and characterisation of hypomethylated DNA loci controlling quantitative resistance in Arabidopsis. eLife, 8. e40655. ISSN 2050-084X

<https://doi.org/10.7554/eLife.40655>

© 2019, Furci et al. This is an author produced version of a paper subsequently published in eLife. Uploaded in accordance with the publisher's self-archiving policy.

Reuse

This article is distributed under the terms of the Creative Commons Attribution (CC BY) licence. This licence allows you to distribute, remix, tweak, and build upon the work, even commercially, as long as you credit the authors for the original work. More information and the full terms of the licence here:
<https://creativecommons.org/licenses/>

Takedown

If you consider content in White Rose Research Online to be in breach of UK law, please notify us by emailing eprints@whiterose.ac.uk including the URL of the record and the reason for the withdrawal request.



eprints@whiterose.ac.uk
<https://eprints.whiterose.ac.uk/>

Identification and characterisation of hypomethylated DNA loci controlling quantitative resistance in Arabidopsis

Leonardo Furci^{1*}, Ritushree Jain^{1*}, Joost Stassen¹, Oliver Berkowitz², James Whelan², David Roquis^{3,4}, Victoire Baillet⁵, Vincent Colot⁵, Frank Johannes^{3,4} & Jurriaan Ton^{1*}

¹ P³ Centre for Translational Plant & Soil Biology, Department of Animal & Plant Sciences, University of Sheffield, UK.

² Department of Animal, Plant and Soil Science, ARC Centre of Excellence in Plant Energy Biology, La Trobe University, Australia.

³ Department of Plant Sciences, Technical University of Munich, Liesel-Beckmann-Str. 2, Freising 85354, Germany.

⁴ Institute for Advanced Study (IAS), Technical University of Munich, Lichtenbergstr. 2a, Garching 85748, Germany.

⁵ *Institut de Biologie de l'Ecole Normale Supérieure (IBENS), Ecole Normale Supérieure, Centre National de la Recherche Scientifique (CNRS), Institut National de la Santé et de la Recherche Médicale (INSERM), PSL Université Paris, France.*

* equal contributions

Competing financial interests:

The authors declare no competing financial interests.

Word count:

Abstract: **149**

Main text: **5133**

Methods: **2877**

Abstract

Variation in DNA methylation enables plants to inherit traits independently of changes to DNA sequence. Here, we have screened an Arabidopsis population of epigenetic recombinant inbred lines (epiRILs) for resistance against *Hyaloperonospora arabidopsidis* (Hpa). These lines share the same genetic background, but show variation in heritable patterns of DNA methylation. We identified 4 epigenetic quantitative trait loci (epiQTLs) that provide quantitative resistance without reducing plant growth or resistance to other (a)biotic stresses. Phenotypic characterisation and RNA-sequencing analysis revealed that Hpa-resistant epiRILs are primed to activate defence responses at the relatively early stages of infection. Collectively, our results show that hypomethylation at selected pericentromeric regions is sufficient to provide quantitative disease resistance, which is associated with genome-wide priming of defence-related genes. Based on comparisons of global gene expression and DNA methylation between the wild-type and resistant epiRILs, we discuss mechanisms by which the pericentromeric epiQTLs could regulate the defence-related transcriptome.

Introduction

Eukaryotic cytosine methylation plays an important role in the regulation of gene expression and genome stability. In plants, this form of DNA methylation occurs at three sequence contexts: CG, CHG and CHH, where H indicates any base except guanine (G)^{1,2}. Patterns of plant DNA methylation in the plant genome can remain stable over multiple generations and influence heritable phenotypes³. Recent evidence has suggested that reduced DNA methylation increases the responsiveness of the plant immune system⁴. This ‘priming’ of plant defence enables an augmented induction of defence-related genes after pathogen attack, causing increased levels of quantitative resistance⁵⁻⁸. In some cases, priming of defence-related genes is associated with post-translational histone modifications that mark a more open chromatin structure^{9,10}. Additional evidence for epigenetic regulation of plant immunity has come from independent studies reporting that disease-exposed *Arabidopsis* produces progeny that expresses transgenerational acquired resistance (TAR), which is associated with priming of defence-related genes^{10,11}. Furthermore, *Arabidopsis* mutants that are impaired in the establishment or maintenance of DNA methylation mimic TAR-related priming without prior priming stimulus¹²⁻¹⁴. By contrast, the hyper-methylated *ros1-4* mutant, which is impaired in active DNA de-methylation, is more susceptible to biotrophic pathogens, affected in defence gene responsiveness, and impaired in TAR^{14,15}. Thus, DNA (de)methylation determines quantitative disease resistance by influencing the responsiveness of defence-related genes. However, causal evidence that selected hypomethylated DNA loci are responsible for the meiotic transmission of this form of quantitative disease resistance is lacking.

Epigenetic Recombinant Inbred Lines (epiRILs) have been developed with the aim to study the epigenetic basis of heritable plant traits^{16,17}. EpiRILs show little differences in DNA sequence, but vary substantially in DNA methylation. A commonly used population of epiRILs is derived from a cross between the *Arabidopsis* wild-type (Wt) accession Col-0 and the decreased DNA methylation1-2 (*ddm1-2*) mutant¹⁷. The DDM1 protein is a chromatin remodelling enzyme that provides DNA methyltransferase enzymes access to heterochromatic transposable elements (TEs)¹⁸⁻²⁰. Accordingly, the *ddm1-2* mutation causes loss of pericentromeric heterochromatin and reduced DNA methylation in all sequence contexts^{21,22}. Although the epiRILs from the *ddm1-2* x Col-0 cross do not carry the *ddm1-2* mutation, they contain stably inherited hypomethylated DNA regions from the *ddm1-2* parent, which are maintained up to 16 generations of self-pollination^{17,23,24}. A core set of 123 epiRILs from this

population at the 8th generation of self-pollination in the wild-type (Wt) background has been characterized for differentially methylated region (DMR) markers, enabling linkage mapping of heritable hypomethylated loci controlling root growth, flowering and abiotic stress tolerance^{8,25,26}.

In this study, we have characterised the core set of 123 lines from the *ddm1-2* x Col-0 *epiRIL* population for resistance against the biotrophic downy mildew pathogen *Hyaloperonospora arabidopsidis* (Hpa) to search for heritable hypomethylated loci controlling disease resistance. We identified 4 of these epigenetic quantitative trait loci (*epiQTLs*), accounting for 60% of the variation in disease resistance. None of these *epiQTLs* were associated with growth impairment, indicating that the resistance does not incur major physiological costs on plant development. Further phenotypic characterisation and transcriptome analysis of selected Hpa-resistant *epiRILs* revealed that their resistance is associated with genome-wide priming of defence-related genes. Interestingly, bisulfite sequencing did not reveal defence regulatory genes inside the *epiQTL* regions that were simultaneously primed and hypomethylated, suggesting that DDM1-dependent DNA methylation at the *epiQTLs* trans-regulates the responsiveness of distant defence genes.

Results

Identification of *epiQTLs* controlling quantitative resistance against *Hpa*.

To examine the role of DDM1-dependent DNA methylation in heritable disease resistance, 123 *epiRILs* from the *ddm1-2* x Col-0 cross were analysed for Hpa resistance and compared to siblings of the *ddm1-2* parent (Figure 1a, red), the Wt parent (Col-0), and five progenies thereof (Figure 1a, green). Leaves of three-week old plants were inoculated with Hpa conidiospores and then collected for trypan-blue staining at six days post inoculation (dpi). Microscopic classification of leaves into 4 classes of Hpa colonisation (Figure 1-figure supplement 1) revealed 51 *epiRILs* with statistically enhanced levels of resistance compared to each susceptible Wt line (Pearson's Chi-squared tests, $p < 0.05$). Of these, 8 *epiRILs* showed similar levels of Hpa resistance as the *ddm1-2* line (Figure 1a, dark blue triangles; Pearson's Chi-squared test, $p > 0.05$), whereas 43 *epiRILs* showed intermediate levels of resistance. To identify the *epiQTL(s)* responsible for the observed variation in Hpa resistance, the categorical classification of Hpa infection was converted into a single value numerical resistance index

(RI; Figure 1a, bottom graph). Using a linkage map of stably inherited DMR markers²³ (Supplementary dataset S1), interval mapping revealed 4 statistically significant epiQTLs on chromosomes I, II, IV and V (Figure 1b). The epiQTL on chromosome II had the highest logarithm of odds (LOD) value. For all epiQTLs, the DMR markers with the highest LOD scores ('peak markers') showed a positive correlation between ddm1-2 haplotype and RI (Figure 1c), indicating that the hypomethylated haplotype from ddm1-2 increases resistance against Hpa. A linear regression model to calculate the percentage of RI variance explained by each peak marker ($R^2(g)$)²⁵ confirmed that the DMR peak marker of the epiQTL on chromosome II had the strongest contribution to RI variation. Using an additive model, the combined contribution of all epiQTL peak markers to RI variation ($R^2(G)$)²⁵ was estimated at 60.0% (Figure 1d).

DNA methylation maintains genome stability by preventing transposition of TEs. In the Col-0 x ddm1-2 epiRIL population, reduced methylation at the ddm1-2 haplotype occurs predominantly at long transposons in heterochromatic pericentromeric regions^{20,23}. Frequent transposition events in the epiRILs are nevertheless rare as most DNA hypomethylation occurs at relic transposons that have lost the ability to transpose, and the occurrence of independent transposition events at similar loci is extremely unlikely^{23,27}. However, it is possible that transposition events originating from the heavily hypomethylated ddm1-2 parent were crossed into the population, resulting into shared transposition events (STEs) between multiple epiRILs, which could have contributed to variation in resistance. To account for this possibility, we compared the genomic DNA sequences of the 4 epiQTL intervals from 122 epiRILs (LOD drop-off = 2) for the presence of STEs in more than two epiRILs, using TE-tracker software²⁸. This analysis revealed three STEs in the epiQTL interval on chromosome I (Supplementary dataset S2), while no STEs could be detected in the other epiQTL intervals. None of the STEs in the epiQTL on chromosome I showed statistically significant linkage with RI (Supplementary dataset S2). Accordingly, we conclude that the segregating Hpa resistance in the epiRIL population is caused by epigenetic variation in DNA methylation, rather than genetic variation by STEs.

Effects of the resistance epiQTLs on plant growth and resistance against other (a)biotic stresses.

Expression of inducible defence mechanisms is often associated with physiological costs, resulting in reduced plant growth²⁹. To determine whether the resistance that is controlled by the 4 epiQTLs is associated with costs to plant growth, we quantified the green leaf area (GLA) of 12-15 individual plants per line at the stage of Hpa inoculation (Figure 1-figure supplement 2). Subsequent interval mapping revealed one statistically significant epiQTL on chromosome I (Figure 1b). The corresponding peak marker (MM150) showed a negative correlation between GLA and ddm1-2 haplotype (Figure 1c), indicating that the hypomethylated ddm1-2 allele at this locus represses plant growth. The growth epiQTL mapped to a different region than the resistance epiQTL on chromosome I (Figure 1b, inset). Furthermore, none of the 8 most resistant epiRILs showed significant growth reduction compared to all Wt lines in the screen (Figure 1-figure supplement 2). Hence, the resistance provided by the 4 hypomethylated epiQTLs is not associated with major physiological costs to plant growth.

Enhanced defence to one stress can lead to enhanced susceptibility to another stress, which is caused by antagonistic cross-talk between defence signalling pathways³⁰. To examine whether Hpa resistance in the epiRIL population is associated with increased susceptibility to other stresses, we compared the 8 most Hpa-resistant epiRILs (Figure 1a; Figure 1-figure supplement 3a) for resistance against the necrotrophic fungus *Plectosphaerella cucumerina* (Pc) and tolerance to salt (NaCl). At nine dpi with Pc spores, epiRIL#193 showed a statistically significant reduction in necrotic lesion size compared to the Wt (line #602), indicating enhanced resistance (Figure 1-figure supplement 3b). The seven other epiRILs showed unaffected levels of Pc resistance that were similar to the Wt. Salt tolerance was quantified by the percentage of seedlings with fully developed cotyledons at six days after germination on agar medium with increasing NaCl concentrations. Remarkably, all Hpa-resistant epiRILs showed varying degrees of tolerance to the highest NaCl concentration compared to Wt plants (Figure 1-figure supplement 3c). Thus, the quantitative resistance to Hpa in the epiRIL population does not compromise resistance against necrotrophic pathogens or abiotic stress.

***Hpa*-resistant epiRILs are primed to activate different defence mechanisms.**

Basal resistance against Hpa involves a combination of salicylic acid (SA)-dependent and SA-independent defence mechanisms^{31,32}. To examine the role of SA-dependent defences, we

183 profiled the expression of the SA-inducible marker gene PR1 at 48 and 72 hours post
184 inoculation (hpi), which represents a critical time-window for host defence against Hpa^{33,34}.
185 None of the epiRILs showed a statistically significant increase in basal PR1 expression after
186 mock inoculation (Figure 2a; Figure 1-figure supplement 4a), indicating that the resistance is
187 not based on constitutive up-regulation of SA-dependent defence signalling. However, in
188 comparison to the Wt line, epiRILs #71, #148, #193, #229 and #508 showed augmented
189 induction of PR1 at 48 and/or 72 hpi with Hpa (Figure 2a; Figure 1-figure supplement 4a),
190 indicating priming of SA-inducible defences⁷. To assess the role of cell wall defence, all lines
191 were analysed for effectiveness of callose deposition, which is a pathogen-inducible defence
192 mechanism that is largely controlled by SA-independent signalling³⁵. Compared to the Wt line,
193 all but one epiRIL (#193) showed a statistically significant increase in the proportion of callose-
194 arrested germ tubes (Figure 2a; Figure 1-figure supplement 4b). Hence, the 8 most Hpa-
195 resistant epiRILs are primed to activate differentially regulated defence responses, which
196 explains the lack of major costs on growth and compatibility with other types of (a)biotic stress
197 resistance in the epiRILs (Figures 1b and 2a; Figure 1-figure supplements 2-4).

199 **Transgenerational stability of the resistance.**

200 The 123 epiRILs analysed for Hpa resistance had been self-pollinated for 8 generations in a
201 Wt (Col-0) genetic background since the F1 x Col-0 backcross (F9)¹⁷. To examine the
202 transgenerational stability of the resistance phenotype over one more generation, 5 individuals
203 from the 8 most resistant epiRILs and the Wt line (Figure 1a, Figure 1-figure supplement 3a)
204 were selected to generate F10 families, which were then tested for Hpa resistance. Comparing
205 distributions of pooled leaves from all five families per line confirmed that each epiRIL
206 maintained a statistically enhanced level of resistance (Figure 1-figure supplement 5; Pearson's
207 Chi-squared test, $p < 0.05$; top asterisks). However, when comparing individual F10 families to
208 the Wt, 2 of the 40 F10 families (line #71-2 and line #148-2) exhibited Wt levels of
209 susceptibility, indicating that they had lost Hpa resistance from the F9 to the F10 generation.
210 Furthermore, 4 of the 8 epiRILs tested (#71, #148, #545, and #508) displayed statistically
211 significant variation in Hpa resistance between the 5 F10 families within the epiRIL (Figure 1-
212 figure supplement 5; Pearson's Chi-squared test, $p < 0.05$; † symbols), suggesting instability of
213 the Hpa resistance.

***Hpa*-resistant epiRILs show genome-wide priming of defence-related genes.**

To study the transcriptomic basis of the transgenerational resistance, Wt plants (line #602) and 4 Hpa-resistant epiRILs (#148, #193, #454 and #508), each carrying different combinations of the 4 epiQTLs, were analysed by RNA sequencing at 48 and 72 hpi (Figure 2a, bottom panel). Principal component analysis (PCA) of biologically replicated samples ($n = 3$) revealed clear separation between all treatment/time-point/epi-genotype combinations (Figure 2b). The first PCA axis explained 31% of the variation in transcript abundance, separating samples from mock- and Hpa-treated plants, whereas the second PCA axis explained 20% of the variation, mostly separating samples from the different lines (Figure 2b). This PCA pattern indicates that the response to Hpa infection had a bigger effect on global gene expression than epi-genotype. Moreover, samples from Hpa-inoculated epiRILs showed relatively little difference between both time-points (Figure 2b), whereas samples from Hpa-inoculated Wt plants at 48 hpi clustered between samples from mock-inoculated Wt plants and samples from Hpa-inoculated Wt plants at 72 hpi. This pattern suggests a difference in the speed and/or intensity of the transcriptional response to Hpa. To explore this possibility further, we performed three-factorial likelihood ratio tests ($q < 0.05$) to select differentially expressed genes between all epigenotype/treatment/time-point combinations. This analysis identified 20,569 genes, representing 61% of all annotated RNA-producing genes in the Arabidopsis genome, including transposable elements, non-coding RNA genes and pseudogenes (Supplementary dataset S3). Of these, 9,364 genes were induced by Hpa at 48 and/or 72 hpi in one or more lines (Supplementary dataset S4). Subsequent hierarchical clustering of this gene selection revealed a large cluster of Hpa-inducible transcripts displaying augmented induction in the epiRILs at the relatively early time-point of 48h after Hpa inoculation (Figure 2-figure supplement 1).

To characterize further the pathogen-inducible transcriptome of the resistant epiRILs, we selected Hpa-inducible genes showing elevated levels of expression in the epiRILs during Hpa infection. Within this gene selection, we distinguished two expression profiles. The first group of genes had been selected for constitutively enhanced expression in the resistant epiRILs, using the following criteria (Wald tests, $q < 0.05$): i) Hpa-inducible in the Wt, ii) not inducible by Hpa in the epiRIL and iii) displaying enhanced accumulation in mock-treated epiRIL that is equal or higher than accumulation in the Hpa-inoculated Wt ('Group 1'; Figure 2-figure supplement 2a). The second group of genes had been selected for enhanced Hpa-induced expression in the epiRILs, using the following criteria (Wald tests, $q < 0.05$): i) Hpa-inducible in the Wt (#602), ii) Hpa-inducible in the epiRIL(s) and iii) displaying statistically

increased accumulation in Hpa-inoculated epiRILs compared to Hpa-inoculated Wt plants ('Group 2'; Figure 2-figure supplement 2a). For each epiRIL, we identified more genes in Group 2 than in Group 1 (Figure 2c; Figure 2-figure supplements 2b, 3 and 4; Supplementary datasets S5 and S6). This difference was most pronounced at 48 hpi, which represents a critical time-point for host defence against Hpa^{33,34}. Analysis of a statistical interaction between epi-genotype x Hpa treatment revealed that > 92% of all genes in Group 2 are significant for this interaction term (Supplementary dataset S7), indicating a constitutively primed expression pattern. Visualisation of the expression profiles in heatmaps confirmed this notion, showing that the induction of Group 2 genes by Hpa is strongly augmented in the resistant epiRILs compared to the Wt line (Figure 2c; Figure 2-figure supplement 4), which is consistent with the definition of plant defence priming⁷.

To examine the functional contributions of the Hpa-inducible genes in Groups 1 and 2, we employed gene ontology (GO) term enrichment analysis. After exclusion of redundant GO terms³⁶, we identified 469 GO terms, for which one or more of the sets showed statistically significant enrichment. Group 2 genes at 48 hpi displayed dramatically enhanced GO term enrichment compared to all other sets, which was obvious for all epiRILs (Figure 2d). This enrichment was particularly pronounced for 111 GO terms relating to SA-dependent and SA-independent defence mechanisms (Supplementary dataset S8), which supports our phenotypic characterisation of SA-dependent and SA-independent defence markers (Figure 1-figure supplement 4). Collectively, these results suggest that the quantitative resistance of the epiRILs is based on priming of Hpa-inducible defence genes.

Interestingly, compared to the other gene selections, a relatively large proportion of defence-related genes in Group 2 at 48 hpi was shared between all 4 epiRILs (Figure 2-figure supplement 2b), pointing to relatively high similarity in the augmented immune response of the epiRILs. Furthermore, only 5% of the genes in the Group 1 and 6.5% of the genes in Group 2 are physically located within the borders of the epiQTL intervals (LOD drop-off = 2). The frequency of Group 1 and 2 genes relative to all other genes was significantly lower for the epiQTL regions compared to the entire Arabidopsis genome (14.6%; Pearson's Chi-squared test, $p < 0.05$). Thus, the majority of Hpa-inducible Group 1 and 2 genes showing enhanced expression in the more resistant epiRILs are (trans-)regulated by DNA methylation at the 4 epiQTLs.

The resistance epiQTLs do not contain defence genes that are *cis*-regulated by DNA methylation, suggesting involvement of *trans*-regulatory mechanisms.

Although 92% of all genes in Group 2 were located outside the physical borders of the 4 epiQTL intervals (LOD-drop-off = 2), we hypothesized that a small set of defence regulatory genes inside the epiQTL regions are directly (*cis*-)regulated by DNA methylation to mediate augmented levels of defence in response to Hpa infection. Since the Group 2 genes were strongly enriched with defence-related GO terms (Figure 2d), we examined whether their augmented expression during Hpa infection is associated with the hypomethylated *ddm1-2* haplotype. To this end, we calculated for each gene in Group 2 the ratio of normalized transcript abundance between Hpa-inoculated epiRIL and the Hpa-inoculated Wt line, which is proportional to their level of augmented expression during Hpa infection. Hierarchical clustering of these ratios enabled us to select for genes that exclusively show augmented expression when associated with the hypomethylated *ddm1-2* haplotype of the corresponding epiQTL (Figure 3a; Figure 3-figure supplement 1a). The expression ratios of 279 epiQTL-localised genes did not correlate with the *ddm1-2* haplotype (Figure 3a, cluster II; Figure 3-figure supplement 1a; Supplementary dataset S9), indicating that DNA methylation does not *cis*-regulate their augmented Hpa-inducible expression. By contrast, 73 epiQTL-localised genes only showed augmented expression when associated with the hypomethylated *ddm1-2* haplotype (Figure 3a, cluster I; Figure 3-figure supplement 1a; Supplementary dataset S10). To confirm the hypomethylated status of these genes, we performed comprehensive bisulfite sequencing analysis of DNA methylation for the 4 epiRILs and the Wt line. DMR analysis of the gene body (GB), 2kb promoter region (P) and 1kb downstream (D) regions confirmed that the levels of augmented gene expression of the 279 genes in cluster II do not correlate positively with the extent of DNA hypomethylation (Figure 3b, Figure 3-figure supplement 1b). This notion was confirmed by linear regression analysis between the augmented expression ratio (48 hpi) and the average level of DNA hypomethylation (Figure 3-figure supplement 2), indicating that the 279 genes in cluster II are regulated indirectly (in *trans*) by DNA methylation. By contrast, the 73 epiQTL-based genes in cluster I showed a positive correlation between augmented expression ratio (48 hpi) and DNA hypomethylation, which was statistically significant for each epiQTL ($p < 0.05$; Figure 3-figure supplement 2). These results indicate that the 73 genes in cluster I are regulated locally (in *cis*) by DNA methylation.

Nearly all *cis*-regulated genes in cluster I showed a TE-like pattern of DNA methylation in the Wt (teM; methylation at CG, CHG and CHH contexts), whereas most cluster II genes showed

either no methylation or a pattern of gene-body methylation in the Wt (gbM; methylation at CG only; Figure 3b and Figure 3-figure supplement 1b). Furthermore, dividing hypomethylation at gene bodies of Group 2 genes by type of DNA methylation (i.e. either teM or gbM) and plotting these values against augmented expression ratio revealed a statistically significant correlation between expression ratio and reduced teM ($p=1.06e^{-8}$; Figure 3-figure supplement 3), whereas no such correlation was found for reduced gbM ($p=0.66$; Figure 3-figure supplement 3). These results support the growing notion that reduced teM increases gene expression, whereas changes in gbM have no direct influence on gene expression³⁷.

The majority of in cis-regulated genes in cluster I genes were annotated as TEs, such as DNA transposons of the CACTA family, retrotransposons of the GYPSY or COPIA families, or TE-related genes, encoding transposases or enzymes necessary for TE function (Supplementary dataset S10). Only six genes were annotated as protein-coding genes, of which two shared homology to known protein-encoding genes (At2G07240, cysteine-type peptidase; At2G07750, RNA helicase). However, none of these two genes has previously been associated with plant defence. Furthermore, analysis of the genomic context of the six protein-coding genes revealed the presence of overlapping and/or nearby TEs (Figure 3-figure supplement 4), suggesting that their correlation between augmented expression and DNA hypomethylation is determined by association with TEs. Since TE-encoded proteins have no antimicrobial activity or direct defence regulatory function, our results suggest that global defence gene priming by hypomethylated epiQTLs is not based on cis-regulation of defence regulatory genes, but rather on alternative trans-acting mechanisms by DNA methylation of the TE-rich epiQTL.

Discussion

By screening the Col-0 x ddm1-2 epiRIL population for leaf colonisation by the downy mildew pathogen Hpa, we have identified 4 epiQTLs that provide quantitative disease resistance (Figure 1b). The combined contribution of all 4 DMR peak markers was estimated at 60% of the total variation (Figure 1d), which is higher than previously reported variation in developmental plant traits for this population²⁴⁻²⁶. It was previously shown that half of all stably

inherited DMRs in the Col-0 x ddm1-2 epiRILs also occur in natural Arabidopsis accessions^{24,38}. Considering that the epiRIL population includes heritable variation in a range of ecologically important plant traits, including flowering, root growth, nutrient plasticity and (a)biotic stress resistance²⁴⁻²⁶, it is tempting to speculate that variation in DDM1-dependent DNA methylation contributes to natural variation and environmental adaptation of Arabidopsis. Indeed, the phenotypic diversity in the Col-0 x ddm1-2 epiRIL population closely resembles that of natural Arabidopsis accessions^{39,40}. Furthermore, independent studies have shown that high levels of enduring (a)biotic stress can trigger transgenerational acquired resistance (TAR) in Arabidopsis^{10,41,42}. Interestingly, repeated inoculation of 2- to 5-weeks old Arabidopsis seedlings with the hemi-biotrophic leaf pathogen *Pseudomonas syringae* pv. tomato causes TAR, which is associated with reduced transcription of DDM1 gene in local leaves that is maintained in the apical meristem of paternal plants (Furci and Ton, unpublished results). To what extent this prolonged repression in DDM1 gene transcription causes heritable reduction in DNA methylation at the epiQTLs requires further study.

Aller et al. (2018) have recently used the same Col-0 x ddm1-2 epiRIL population to map the contribution of heritable variation in DNA methylation to the production of defence-related glucosinolate metabolites⁴³. Interestingly, the resistance epiQTL on chromosome I from our study partially overlaps with an epiQTL that influences basal production of the aliphatic glucosinolate 3-methylthiopropyl (3MTP)⁴³. Glucosinolates contribute to defence against both herbivores and microbes⁴⁴. Moreover, myrosinase-dependent breakdown products of indole-derived 4-methoxy-indol-3-ylmethylglucosinolate have been linked to the regulation of callose-mediated cell wall defence in Arabidopsis^{45,46}. However, the 3MTP-controlling epiQTL identified by Aller et al. (2018) was relatively weak compared to the epiQTL controlling Hpa resistance (Figure 1b), indicating that its contribution to Hpa resistance would at most be marginal. Furthermore, our transcriptome analysis revealed that the largest variation in gene expression between epiRILs and the Wt line comes from the transcriptional response to Hpa, rather than differences in basal gene expression (Figure 2b-c). Moreover, the genes in Group 2, which displayed enhanced Hpa-induced expression in the resistant epiRILs at the critical early time-point of 48 hpi, were strongly enriched with defence-related GO terms (Figure 2d). The majority of these Group 2 genes showed a statistically significant interaction between epi-genotype and Hpa treatment (Supplementary dataset S7), indicating that these epiRILs were primed to activate defence-related genes. This notion was supported by the actual expression profiles of Group 2 genes (Figure 2c; Figure 2-figure supplement 4), as well as the

defence phenotypes of the 8 most resistant epiRILs in the population (Figure 2a; Figure 1-figure supplement 4). Furthermore, our epiRIL screen for growth phenotypes demonstrated that the resistance-controlling epiQTLs do not have a major impacts on plant growth (Figure 1b), which is consistent with previous findings that defence priming is a low-cost defence strategy⁴⁷. While we cannot exclude other mechanisms, these independent lines of evidence collectively indicate that genome-wide priming of defence genes is the most plausible mechanism by which the epiQTLs mediate quantitative disease resistance in the population.

Over recent years, various studies have established a link between DNA hypomethylation and plant immune priming^{4,6,14}. However, causal evidence that heritable regions of reduced DNA methylation mediate transgenerational disease resistance is lacking. Our study has shown that heritable regions of hypomethylated DNA are sufficient to mediate resistance in a genetic Wt background. Furthermore, our study is the first to link phenotypic and epigenetic variation of selected epiRILs to profiles of global gene expression, revealing that epigenetically controlled resistance is associated with genome-wide priming of defence-related genes (Figure 2b-d; Figure 2-figure supplement 1; Figure 2-figure supplement 4). The majority of these pathogenesis-related genes showed augmented induction at 48 hpi (Figure 2c), which represents a critical early time-point in the interaction between *Arabidopsis* and *Hpa*, during which hyphae from germinating spores start to penetrate the epidermal cell layer and invade the mesophyll^{33,34}. Notably, this set of primed genes was substantially more enriched in SA-dependent and SA-independent defence GO terms than the set of *Hpa*-inducible genes that were constitutively up-regulated in *Hpa*-resistant epiRILs (Figure 2d), corroborating the analysis of phenotypical defence markers (Figure 2a; Figure 1-figure supplement 4).

DNA methylation of TEs has been reported to cis-regulate expression of nearby genes in *Arabidopsis*⁴⁸⁻⁵². By contrast, our study did not find evidence that DNA methylation in the epiQTLs cis-regulates the responsiveness of nearby of defence genes. Firstly, the majority of primed defence genes in the *Hpa*-resistant epiRILs were located outside the epiQTL intervals (92%). Secondly, of all primed genes within the epiQTLs, only 73 showed augmented induction that coincided with DNA hypomethylation (Figure 3a; Figure 3-figure supplement 1; Figure 3-figure supplement 2; Supplementary dataset S10). Of these, 67 encoded TEs or TE-related genes, while the six protein-encoding genes were closely associated with one or more TEs and did not have functions related plant defence (Figure 3a; Figure 3-figure supplement 1; Supplementary dataset S10). Since TEs do not encode defence signalling proteins, we propose that DNA hypomethylation at the TE-rich epiQTLs mediates augmented induction of defence

genes across the genome via trans-acting mechanisms. A recent transcriptome study of Hpa-infected *Arabidopsis* identified 166 defence-related genes that were primed in the hypomethylated *nrpe1-11* mutant and/or repressed in hyper-methylated *ros1-4* mutant¹⁴. The majority of these defence genes were not targeted by NRPE1- and/or ROS1-dependent DNA (de)methylation, indicating that their responsiveness is trans-regulated by DNA methylation. Although NRPE1 and ROS1 target partially different genomic loci than DDM1²⁰, this study supports our hypothesis that DNA methylation controls global defence gene responsiveness via trans-acting mechanisms.

There are various mechanisms by which DNA methylation could trans-regulate defence gene expression. It is possible that transcribed TEs in the hypomethylated epiQTLs generate 21-22nt or 24nt small RNAs (sRNAs) that influence distant heterochromatin formation through via RDR6- and DCL3-dependent RdDM pathways⁵³. Support for trans-regulation by sRNAs came from a recent study, which reported that induction and subsequent re-silencing of pericentromeric TEs in *Arabidopsis* upon *Pseudomonas syringae* infection is accompanied with accumulation of RdDM-related sRNAs that are complementary to TEs and distal defence genes. Interestingly, while the accumulation of these sRNAs coincided with re-silencing of the complementary TEs, the complementary defence genes remained expressed in the infected tissues⁵⁴. These findings are supported by another recent study, which demonstrated that AGO1-associated small RNAs can trans-activate distant defence gene expression through interaction with the SWI/SNF chromatin remodelling complex⁵⁵. Apart from sRNAs, it is also possible that long intergenic noncoding RNAs (lincRNAs) from the hypomethylated epiQTLs regulate pathogen-induced expression of distant defence genes. A recent study revealed that pericentromeric TEs of *Arabidopsis* can produce DDM1-dependent lincRNAs that are increased by abiotic stress exposure⁵⁶. Since lincRNAs can promote euchromatin and heterochromatin formation at distant genomic loci^{57,58}, hypomethylated TEs within the epiQTLs could generate priming-inducing lincRNAs. While knowledge about lincRNAs in plants remains limited, like sRNAs, their activity depends on sequence complementary with target loci⁵⁹. Unlike non-coding RNAs, long-range chromatin interactions can trans-regulate gene expression independently of sequence complementarity⁶⁰⁻⁶³. Previous high-throughput chromosome conformation capture (Hi-C) analysis revealed that the *ddm1-2* mutation has a profound impact on long-range chromatin interactions within and beyond the pericentromeric regions⁶⁴. Projection of these DDM1-dependent interactions onto the *Arabidopsis* genome shows extensive coverage of the resistance epiQTLs identified in this

study (Figure 3-figure supplement 5). Whether these long-range interactions contribute to trans-regulation of defence gene priming would require further study, including a fully replicated Hi-C analysis of the resistant epiRILs characterised in this study.

In conclusion, our study has shown that heritable DNA hypomethylation at selected pericentromeric regions controls quantitative disease resistance in *Arabidopsis*, which is associated with genome-wide priming of defence-related genes. This transgenerational resistance is not associated with reductions in plant growth (Figure 1b), nor does it negatively affect resistance to other types of (a)biotic stresses tested in this study (Figure 1-figure supplement 3). However, whether this form of epigenetically controlled resistance can be exploited in crops depends on a variety of factors, including the stability of the disease resistance and potential non-target effects. For instance, our experiments with *Arabidopsis* revealed that the resistance has limited stability and can erode over one more generation in some epiRILs (Figure 1-figure supplement 5). Furthermore, the genomes of most crop species contain substantially higher numbers of TEs, rendering predictions about the applicability and potentially undesirable side effects on growth and seed production uncertain. Future research will have to point out whether introgression of hypomethylated pericentromeric loci into the background of elite crop varieties allows for selection of meta-stable quantitative disease resistance without side-effects on agronomically important traits.

Methods

Plant material and growth conditions.

Epigenetic recombinant inbred lines (epiRILs) seeds of *Arabidopsis* (*Arabidopsis thaliana*, accession Col-0) were purchased from Versailles *Arabidopsis* Stock Centre, INRA, France (<http://publiclines.versailles.inra.fr/epirils/index>). The epiRIL screen included siblings of the F4 ddm1-2 parental plant of the epiRIL population (IBENS, France). *Arabidopsis* seeds were stratified in water at 4°C in the dark for three-five days. For pathogen bioassays, seeds were sown in a sand:compost mixture (1:3) and grown at short-day conditions for three weeks (8.5 h light/15.5 h dark, 21°C, 80% relative humidity, ~125 $\mu\text{mol s}^{-1} \text{m}^{-2}$ light intensity). To test transgenerational inheritance and stability of Hpa resistance in the 8 most resistant epiRILs (Figure 1-figure supplement 5), 5 individual F9 plants were cultivated for 4 weeks at short-day

conditions and then moved to long-day conditions to initiate flowering (16 h light/8 h dark, 21°C, 80% relative humidity, ~125 $\mu\text{mol s}^{-1} \text{m}^{-1}$ light intensity). Seeds of the 40 F10 families were collected for analysis of Hpa resistance (see below).

Screen for variation in disease resistance and seedling growth.

Three week-old seedlings were spray-inoculated with a suspension of asexual conidia from *Hyaloperonospora arabidopsidis* strain WACO9 (Hpa) at a density of 10^5 spores/ml. Hpa colonization was quantified at six days post inoculation (dpi) by microscopic scoring of leaves, as described previously¹⁴. Briefly, trypan blue-stained leaves were analysed with a stereomicroscope (LAB-30, Optika Microscopes) and assigned to 4 Hpa colonisation classes: class I, no hyphal colonization; class II, $\leq 50\%$ leaf area colonized by pathogen hyphae without formation of conidiophores; class III, $\leq 75\%$ leaf area colonized by hyphae, presence of conidiophores; class IV, $> 75\%$ leaf area colonized by the pathogen, abundant conidiophores and sexual oospores (Figure 1-figure supplement 1). At least 100 leaves per (epi)genotype were analysed, not including the cotyledons. Statistically significant differences in frequency distribution of Hpa colonisation classes between lines were determined by Pearson's Chi-squared tests, using R (v.3.5.1). Growth analysis of the epiRIL population was based on digital photos (Canon 500D, 15MP) of three week-old plants, which were taken on the day of Hpa inoculation. Digital image analysis of total green leaf area (GLA) was performed using Adobe Photoshop 6.0. Green pixels corresponding to GLA were selected and converted into mm^2 after colour range adjustment, using the magic wand tool.

Mapping of epigenetic quantitative trait loci (epiQTLs).

Mapping of epiQTLs was performed using the 'scanone' function of the R/qtl package for R⁶⁵ (Haley-Knott regression, step size: 2cM), combining experimental phenotypical data with the recombination map of differentially methylated regions (DMR) generated previously²³. For analysis of Hpa resistance, the categorical scoring of Hpa resistance was first converted into a numeric resistance index (RI), using the following formula:

$$\text{RI} = (f_{\text{class I}} * 4) + (f_{\text{class II}} * 3) + (f_{\text{class III}} * 2) + (f_{\text{class IV}} * 1),$$

where f = relative frequency of Hpa colonization class of each line, multiplied by an arbitrary weight value ranging from 4 for the most resistant category (class I) to 1 for most susceptible

category (class IV). Mapping of epiQTLs controlling plant growth was based on average GLA values of each line before Hpa infection. A logarithm of odds (LOD) threshold of significance for each trait was determined on the basis of 1,000 permutations for each dataset ($\alpha = 0.05$). The proportion of phenotypic variance $R^2(G)$ explained by the DMR markers with the highest LOD score (peak markers) of all 4 epiQTLs was calculated with the following formula²⁵:

$$R^2(G) = 1 - \frac{n-1}{n-(k+1)} \frac{\sum_i^n (y_i - [\hat{\beta}_0 + \sum_j^k \beta_j g_{ij}])^2}{\sum_i^n (y_i - \bar{y})^2},$$

where n = number of lines analysed, k = number of DMR markers tested; β_0 = intercept of the multiple regression model; β_j = QTL effect for each QTL j (slopes for each marker in the multiple regression model); g_{ij} = (epi) genotype of the jth marker for each individual i (coded as '1' for ddm1-2 epialleles and '-1' for WT epialleles); y_i = phenotypic value of individual i; \bar{y} = mean of phenotypic values. The contribution of each individual QTLj ($R^2(g)$) was calculated, using the following formula:

$$R^2(g) = 1 - \frac{n-1}{n-(k+1)} \frac{\hat{\beta}_j^2 \sum_i^n (g_{ij} - \bar{g}_j)^2}{\sum_i^n (y_i - \bar{y})^2},$$

as described by ²⁵, where n= number of lines analysed, k= number of markers tested; β_j = QTL effect for each QTLj (slopes for each peak marker in the multiple regression model); g_{ij} = (epi)genotype of the jth marker for each individual i (coded as '1' for ddm1-2 epialleles and '-1' for WT epialleles); \bar{g}_j = average of the (epi)genotypes values for the jth marker. Covariance was calculated by subtracting the sum of the individual contributions of each QTLj on phenotypical variance (i.e. $R^2(g_{QTL1}) + R^2(g_{QTL2}) + R^2(g_{QTL4}) + R^2(g_{QTL5})$) from the phenotypical variance explained by the full model (i.e. $R^2(G)$).

Analysis of shared transposition events.

TE-tracker software was used to interrogate available Illumina whole-genome sequencing data from 122 epiRILs for the presence of >2 shared transposition events (STEs) within the epiQTLs intervals²⁸. STEs were analysed for statistically significant linkage with resistance phenotypes (RIs), using the same linear regression model as described above for DMR linkage analysis.

***Plectosphaerella cucumerina* pathoassays.**

Plectosphaerella cucumerina (Pc, strain BMM⁶⁶) was grown from frozen agar plugs (-80° C) on potato dextrose agar (PDA; Difco, UK). Inoculated plates were maintained at room temperature in the dark for at least two weeks. Spores were gently scraped from water-inundated plates, after which spore densities were adjusted to 10⁶ spores/ml using a hemocytometer (Improved Neubauer, Hawksley, UK). Four fully expanded leaves of similar age from five weeks-old plants were inoculated by applying 5µl droplets, minimizing variability due to age-related resistance. After inoculation, plants were kept at 100% RH until scoring of lesion diameters. Average lesion diameters at nine dpi were based on 4 leaves per plant from 12 plants per (epi)genotype (n=40-48), using a precision caliper (Traceable, Fischer Scientific). Statistically significant differences in necrotic lesions diameter (asterisks) were quantified by two-tailed Student's t-test (p<0.05) in pairwise comparisons with Wt line (#602), using R (v3.5.1).

Salt stress tolerance assays.

Seeds were sterilised by exposure for 4 hours (h) to chlorine vapours from a 200ml bleach solution containing 10% v/v hydrochloric acid (37% v/v HCl, Fischer Scientific, 7732-18-5). Seeds were air-dried for one hour in a sterile laminar flow cabinet and plated on half strength MS plates (Duchefa, M0221; +0.05% w/v MES, +1% w/v sucrose, pH 5.7), containing increasing concentrations of NaCl (0mM, 50mM, 75mM and 100mM; Fischer Scientific, 7647-14-5). Plates were stratified for 4 days in the dark at 4°C and transferred to short-day growth conditions (8.5h light/15.5h dark, 21°C, 80% RH, light intensity 100-140 µmol s⁻¹ m⁻¹). Salt tolerance was expressed as percentage of seeds producing fully expanded cotyledons by six days after stratification. Germination percentages of epi-genotypes were calculated from >50 seeds per treatment. Statistically significant differences in germination rates (asterisks) were quantified by Fisher's exact test (p<0.05) in pairwise comparisons with Wt line (#602) at each salt concentration, using R (v3.5.1).

Quantification of callose effectiveness against *Hpa* infection.

Seedlings were collected at three dpi and cleared for >24 h in 100% ethanol. One day prior to analysis, samples were incubated for 30 min in 0.07 M phosphate buffer (pH 9), followed by 15 min incubation in a 4:1 mixture (v/v) of 0.05% w/v aniline blue (Sigma-Aldrich, 415049) in 0.07M phosphate buffer (pH 9) and 0.025% w/v calcofluor white (Fluorescent brightener

28, Sigma-Aldrich, F3543) in 0.1M Tris-HCL (pH 7.5). After initial staining, samples were incubated overnight in 0.5% w/v aniline blue (Sigma-Aldrich, 415049) in 0.07M phosphate buffer (pH 9) and scored with an epifluorescence microscope (Olympus BX 51) fitted with blue filter (XF02-2; excitation 330nm, emission 400nm). Germinated conidia (germ tubes) were divided between in two classes: non-arrested and arrested by callose. In each assay, 10 leaves from different plants for each (epi)genotype were analysed, amounting to >150 conidia-callose interactions. Statistically significant differences in resistance efficiency of callose (asterisks) were analysed using Pearson's Chi-squared tests ($p < 0.05$) in pairwise comparisons with Wt line (#602), using R (v3.5.1).

Reverse-transcriptase quantitative polymerase chain reactions (RT-qPCR).

Three biologically replicated samples for each genotype/treatment/time-point combination were collected at 48 and 72 hpi, each consisting of six to 12 leaves collected from different plants per pot. Samples were snap-frozen in liquid nitrogen and ground to a fine powder, using a tissue lyser (QIAGEN TissueLyser). Total RNA was extracted using a guanidinium thiocyanate-phenol-chloroform extraction isolation protocol. Frozen powder was vortexed for 30 seconds in 1ml Extraction buffer: 1M guanidine thiocyanate (Amresco, 0380), 1M ammonium thiocyanate (Sigma-Aldrich, 1762-95-4), 0.1M sodium acetate (Fisher Scientific, 127-09-3), 38% v/v AquaPhenol (MP Biomedicals, 108-95-2) and 5% v/v glycerol (Fisher Scientific, 56-81-5). Samples were incubated at room temperature (RT) for one min and then centrifuged for five min at 16,500 g. The supernatant was then transferred to a new tube, mixed with 200µl chloroform and vortexed for 10-15 sec. After centrifuging for five min (16,500 g), the aqueous phase was transferred to new tubes, gently mixed by inversion with 350µl 0.8M sodium citrate (Sigma-Aldrich, 6132-04-3) and 350µl isopropanol (Fischer Chemicals, 67-63-0) and left at RT for 10 min for RNA precipitation. Samples were centrifuged for 15 min at 16,500 g (4°C), after which pellets were washed twice in 1ml 70% ethanol, centrifuged at 16,500 g for 1 min, and air-dried before dissolving in 50µl nuclease-free water. Total RNA was quantified, using a Nanodrop 8000 Spectrophotometer (Thermo Scientific). RNA extracts were treated with DNaseI, using the RQ1 RNase-Free DNase kit (Promega, M6101). First-strand cDNA synthesis was performed from 1µg RNA, using SuperScript III Reverse Transcriptase (Invitrogen, 18080093) according to the supplier's recommendations. The qPCR reactions were carried out with a Rotor-Gene Q real-time PCR cycler (Qiagen) and the Rotor-Gene SYBR Green PCR Kit (Qiagen, 204074). Relative PR1 gene expression was calculated, using

Livak's $\Delta\Delta CT$ method⁶⁷ with correction for average PCR efficiencies for each primer pair across experiment samples. Gene expression was normalised against average expression values of At1G13440 (GAPDH), At5G25760 (UBC) and At2G28390 (SAND family protein)⁶⁸. Reactions were performed using previously described primer sequences¹⁴. Statistically significant differences in relative expression (asterisks) were quantified by two-tailed Student's t-test ($p < 0.05$) in pairwise comparisons with Hpa-treated Wt line (#602).

Transcriptome analysis.

Samples for RNA sequencing were collected at 48 and 72 hpi of three week-old plants. Every epi-genotype/treatment/time-point combination was based on three biologically replicated samples, each consisting of 6-12 shoots from different plants. Initial RNA extraction was performed as described for RT-qPCR reactions. Prior to library preparation, RNA concentration and integrity were measured, using 2100 Bioanalyzer (Agilent) with provided reagents kits and according to manufacturer's instructions. All RNA samples had RNA integrity numbers (RIN) > 7.5 . Sequencing libraries were prepared from total RNA, using the TruSeq Stranded Total RNA kit and Ribo-Zero Plant leaf kit (Illumina, RS-122-2401), according to the manufacturer's instructions. Sequencing runs were performed on a HiSeq1500 platform (Illumina), generating paired-end reads of 125 bp and an average quality score (Q30) $> 93\%$. Each sample generated around 35 million paired reads.

Read quality was assessed by FastQC software⁶⁹. Read length and distribution were optimized and adapter sequences were trimmed, using Trimmomatic software⁷⁰. Reads were aligned and mapped to the Arabidopsis genome (TAIR10 annotation), using splice site-guided HISAT2 alignment software (John Hopkins University, second iteration of ⁷¹). For all samples, more than 95% of reads could successfully be mapped once or more onto the Arabidopsis genome. Number of reads per gene were quantified with the Python package HTseq⁷². Differential expression analysis was performed using the DESeq2 R package, which applies a negative binomial generalized linear model to estimate mean and dispersion of gene read counts from the average expression strength between samples⁷³. Prior to principal component analysis (PCA) by the plotPCA function, gene read counts were subjected to regularized logarithmic transformation, using the rlog function⁷³. Likelihood ratio tests of variance within a three-factorial linear model for epigenotype, treatment, time-point and interactions thereof were used to identify genes showing differences in expression across one or more factors⁷³.

Differentially expressed genes (DEGs) were subjected to hierarchical clustering (Ward method) and presented as a heat map, using the pheatmap R package⁷⁴. For each gene, rlog-normalized read counts of each sample were subtracted from the mean of all samples, and divided by the standard deviation to facilitate heatmap visualization (z-score). To identify DEGs between two treatment/time-point/epi-genotype combinations, pair-wise comparisons (Wald test; $q < 0.05$) were performed with the DEGs selection obtained by the lrt test, using the selection criteria illustrated in Figure 2-figure supplement 2a. All Hpa-inducible genes in the Wt and/or epiRILs were selected for elevated expression in the more resistant epiRILs during Hpa infection. Subsequently, these genes were divided between two groups based on their expression profile. Group 1 genes were selected for constitutively enhanced expression in the epiRIL(s) relative to the Wt (Figure 2-figure supplements 2 and 3); Group 2 genes were selected for enhanced levels of Hpa-induced expression in the epiRIL(s) relative to the Wt (Figure 2-figure supplements 2 and 4). To determine the number of Group 2 genes that show a statistically significant interaction between epigenotype x Hpa treatment, all 16,009 genes significant for this interaction were selected from the three-factorial linear model, using the contrast function, and cross-referenced against Group 2 genes.

Gene ontology (GO) term enrichment analysis was performed with the Plant GSEA toolkit⁷⁵. GO terms were checked for significant enrichment against the whole genome background, using a hypergeometric test and Benjamini-Hochberg false discovery rate correction ($q < 0.05$). Lists of enriched GO terms in each treatment were analysed by the GO Trimming 2.0 algorithm³⁶ to remove redundancy of terms, applying a soft trimming threshold of 0.40. The output list from GO Trimming 2.0 was run through GOSlim Viewer (AgBase) to reduce GO terms according to GO slim ontologies (GO consortium). Enrichment was quantified as the percentage of GO term-annotated genes within a certain selection relative to the total number of Arabidopsis genes in that GO term.

Methylome analysis.

For each line, three independent biological replicates were collected, consisting of pooled leaves from six plants of the same developmental stage. High quality genomic DNA was extracted from leaves of five week-old plants, using the GenElute™ Plant Genomic DNA Miniprep Kit (Sigma-Aldrich). Bisulfite sequencing was performed by GATC Biotech (UK). After quality trimming of read sequences, adapter sequences were removed, and reads were

663 filtered by Cutadapt (version 1.9; Pair end-mode; phred score = 20, min.length = 40). Reads
664 were mapped to an index genome, using of BS-Seeker2 (version 2.0.10, mismatch = 0.05,
665 maximum insert size =1000 bp). Bowtie2 (version 2.2.2) was used for alignment of reads, as
666 described previously⁷⁶. Differential methylation for promoter regions (-2kb), gene bodies, and
667 downstream regions (+1kb) relative to the Wt was called using methylkit (version 1.0.0;
668 minimum coverage = 5x, q = 0.05). Differentially methylated states were visualised as a heat
669 map, using the ‘pheatmap’ R package (version 1.0.8)⁷⁴.

670 To differentiate Wt methylation states of all epiQTL-based genes in Group 2 (see above), gene
671 bodies of all nuclear genes were categorised between un-methylated, gene body methylated
672 (gbM; CG context only) or TE-like methylated (teM; CHG and/or CHH with or without CG).
673 For each gene containing 20 or more cytosines, methylated and un-methylated cytosine base
674 calls in each context were extracted from the sequence read alignments. Positions with less
675 than 4x coverage were ignored. Methylation patterns were categorised as TE-like if methylated
676 read calls relative to un-methylated read calls in CHG and/or CHH contexts showed a
677 statistically significant increase over average methylation rates of all genes across the genome
678 in the respective context, using the “binom.test” function in R (FDR-adjusted $p < 0.01$). The
679 remaining genes were classified either as gbM if the same test revealed a statistically significant
680 increase in CG context, or as un-methylated if no statistically significant increase in DNA
681 methylation could be detected in any sequence context.

683 **Correlation analysis between gene expression and DNA methylation.**

684 Correlations between augmented expression ratio of Group 2 genes (see Transcriptome
685 analysis) and DNA hypomethylation (CG), were determined by plotting augmented gene ratios
686 at 48 hpi against average hypomethylation compared to Wt (%) across promoter region, gene
687 body, and downstream region (see Methylome analysis). To determine which type of DNA
688 hypomethylation correlates with augmented expression in the epiRILs, hypomethylation at
689 gene bodies of Group 2 genes were divided between teM and gbM and plotted against the
690 corresponding expression ratios at 48 hpi. If hypomethylation occurred at CG context only,
691 genes were classified as being reduced in gene body methylation (gbM); if hypomethylation
692 occurred all three sequence contexts (CG, CHG, CHH), genes were classified as being reduced
693 in TE methylation (teM). Values of gbM hypomethylation were expressed as percentage
694 reduction in GC methylation relative to the Wt; values of teM hypomethylation were expressed

as percentage reduction in all sequence contexts. Linear regression analyses were performed using R software (v.3.5.1).

Hi-C analysis.

HiC sequence libraries SRR1504819 and SRR1504824⁶⁴ were downloaded from NCBI SRA. Sequences were pre-processed and aligned to the TAIR10 Arabidopsis nuclear genome sequence⁷⁷, using HiCUP (0.5.9)⁷⁸ and Bowtie2⁷⁹ (2.2.6). Alignments were filtered and de-duplicated as part of the processing by HiCUP, before being further processed in HOMER⁸⁰ (4.9.1) at 5kb resolution. Differential interactions were assessed reciprocally, using each sample as background (analyzeHiC-ped). Interactions were determined to be potentially dependent on genotype if the absolute z-score of the primary versus the secondary experiment was more than 1. Visualisations were generated using Circos⁸¹ (0.69-5), based on bundled links (-max_gap 10001).

Data availability.

Transcriptome sequencing and bisulfite sequencing reads are available from the European Nucleotide Archive (ENA) under accession code PRJEB26953.

Acknowledgements

We thank David Pardo and Ana Lopez for technical assistance in the lab. We thank the La Trobe University's Genomics Platform for technical support. The research was supported by a consolidator grant from the European Research Council (ERC; no. 309944 "Prime-A-Plant") to J.T., a Research Leadership Award from the Leverhulme Trust (no. RL-2012-042) to J.T. and a BBSRC-IPA grant to J.T. (BB/P006698/1). Work in V. C. group was supported by the Agence Nationale de la Recherche (ANR-09-BLAN-0237 EPIMOBILE). FJ acknowledges support from the Technical University of Munich - Institute for Advanced Study funded by the German Excellent Initiative and the European Seventh Framework Programme under grant agreement no. 291763. FJ is also supported by the SFB/Sonderforschungsbereich924 of the Deutsche Forschungsgemeinschaft (DFG).

Figures

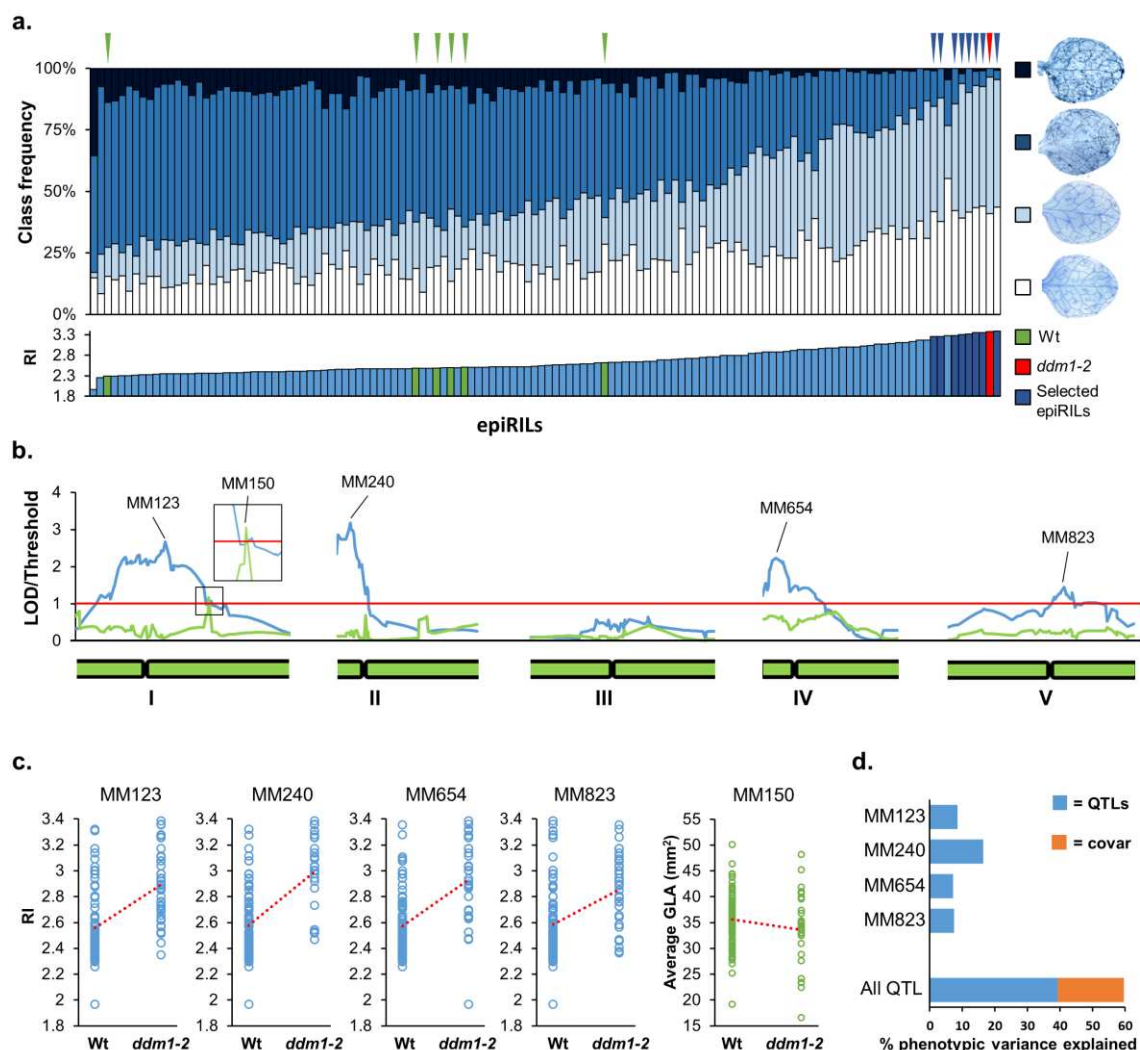
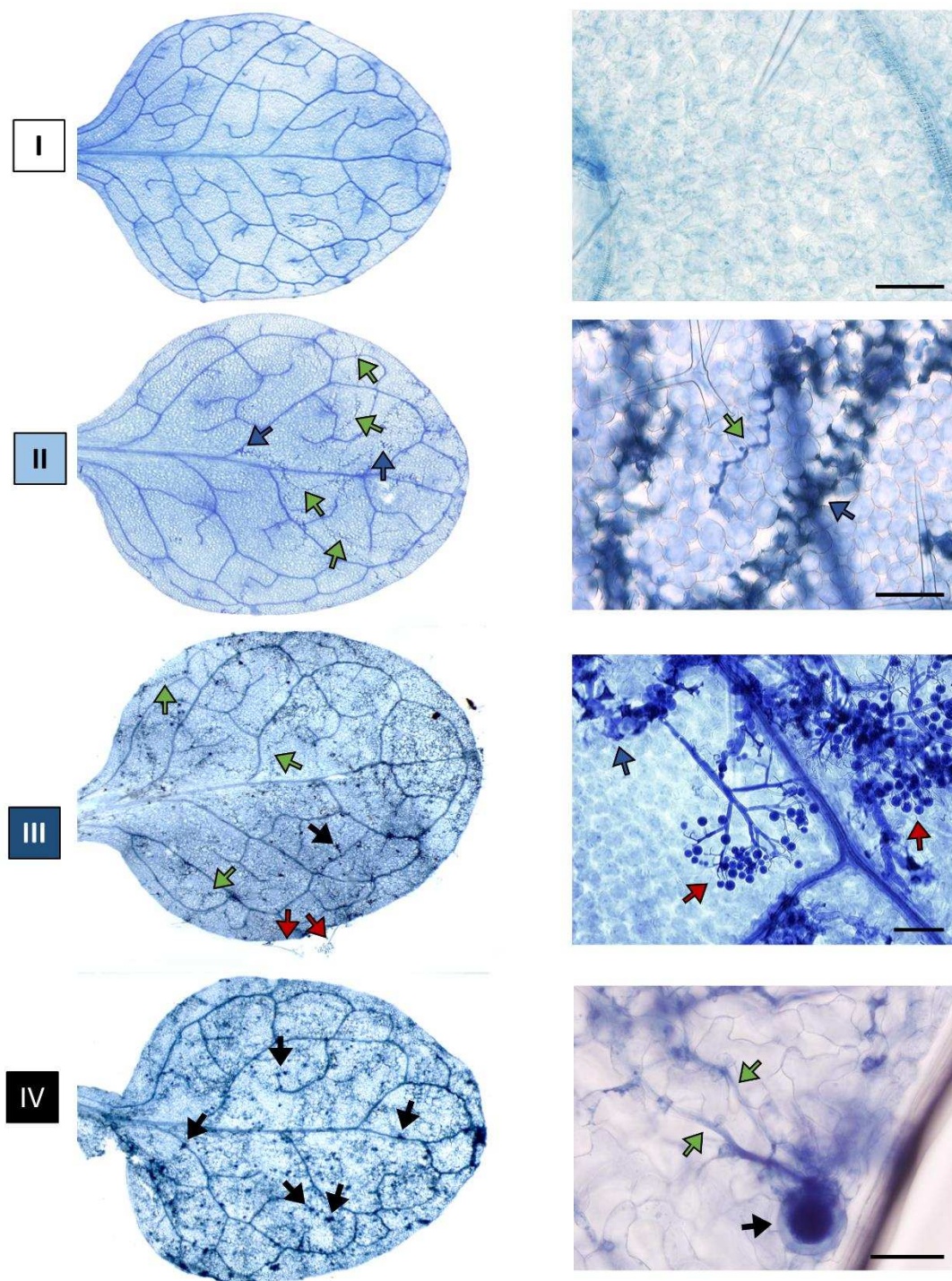


Figure 1. Mapping of epigenetic quantitative trait loci (epiQTL) controlling transgenerational resistance against *Hyaloperonospora arabidopsidis* (Hpa). **a:** Levels of Hpa resistance in 123 epiRIL lines, the ddm1-2 line (F4; red triangle) and six Wt lines (Col-0; green triangles). Top graph shows distribution of infection classes in each epiRIL; blue triangles pinpoint the 8 most resistant epiRILs with statistically similar levels of Hpa colonisation as the ddm1-2 line (Pearson's Chi-squared test, $p > 0.05$). Bottom graph shows variation in Hpa resistance index (RI). Green bars: Wt lines; red bar: ddm1-2; blue bars 8 most resistant epiRILs ($n > 100$). **b:** Linkage analysis of RI (blue line) and green leaf area (GLA) of three-week-old seedlings (green). Green bars at the bottom represent chromosomes. Red line represents the threshold of significance. Peak DMR markers with the highest LOD scores are shown on top. **c:** Correlation plots between peak marker haplotype (methylated Wt versus hypomethylated ddm1-2) and RI (blue) or GLA (green). **d:** Percentages of resistance variance explained by the peak DMR markers, including covariance between markers (orange).



739

740

741

742

743

744

745

746

747

Figure 1-figure supplement 1: Representative examples of infection classes used for quantification of Hpa resistance. Shown are trypan blue-stained Arabidopsis leaves at six days after spray-inoculation with Hpa. White (class I), absent or minimal colonisation; light blue (class II), $\leq 50\%$ leaf area colonised by the pathogen; dark blue (class III), $\leq 75\%$ leaf area colonised by the pathogen, presence of conidiophores; black (class IV), $> 75\%$ leaf area colonised by the pathogen, conidiophores and abundant sexual spores. Green arrows indicate colonisation by pathogen hyphae; blue arrows indicate hyphae surrounded by trailing necrosis, red arrows indicate conidiophores, black arrows indicate sexual oospores. Insets on the right show higher magnifications of colonisation markers. Scale bar = $50\mu\text{m}$.

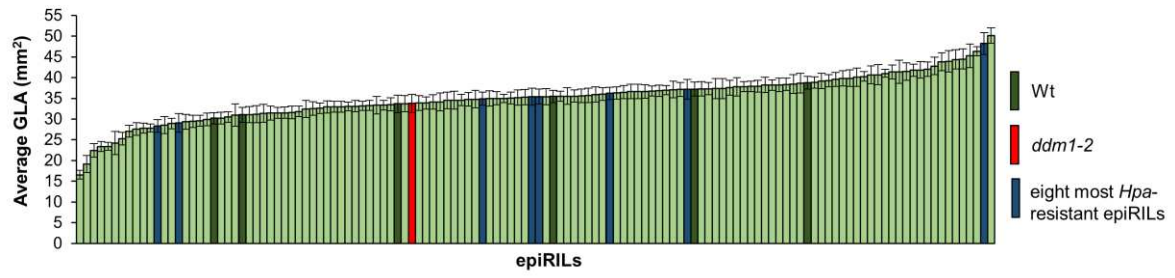
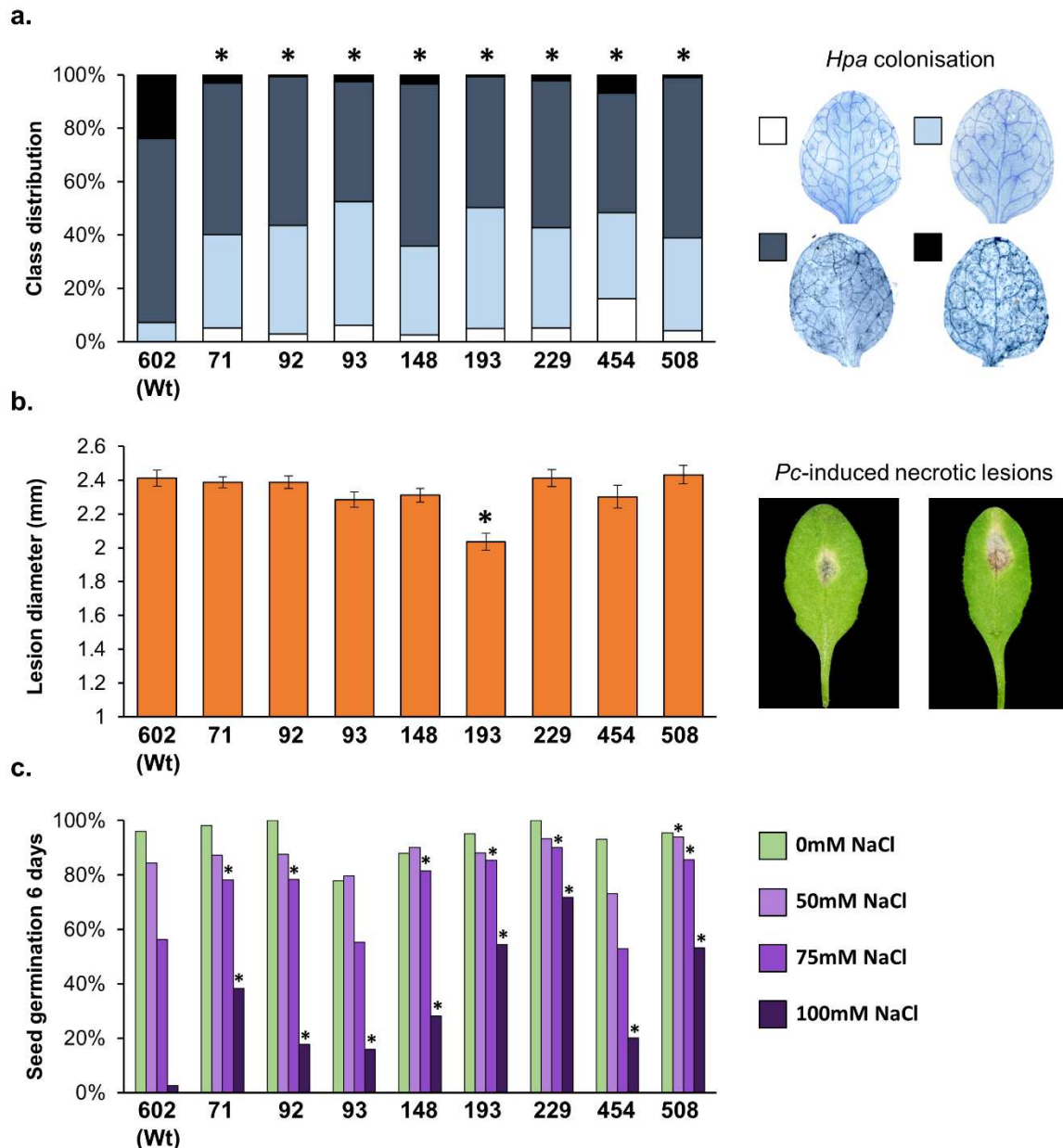
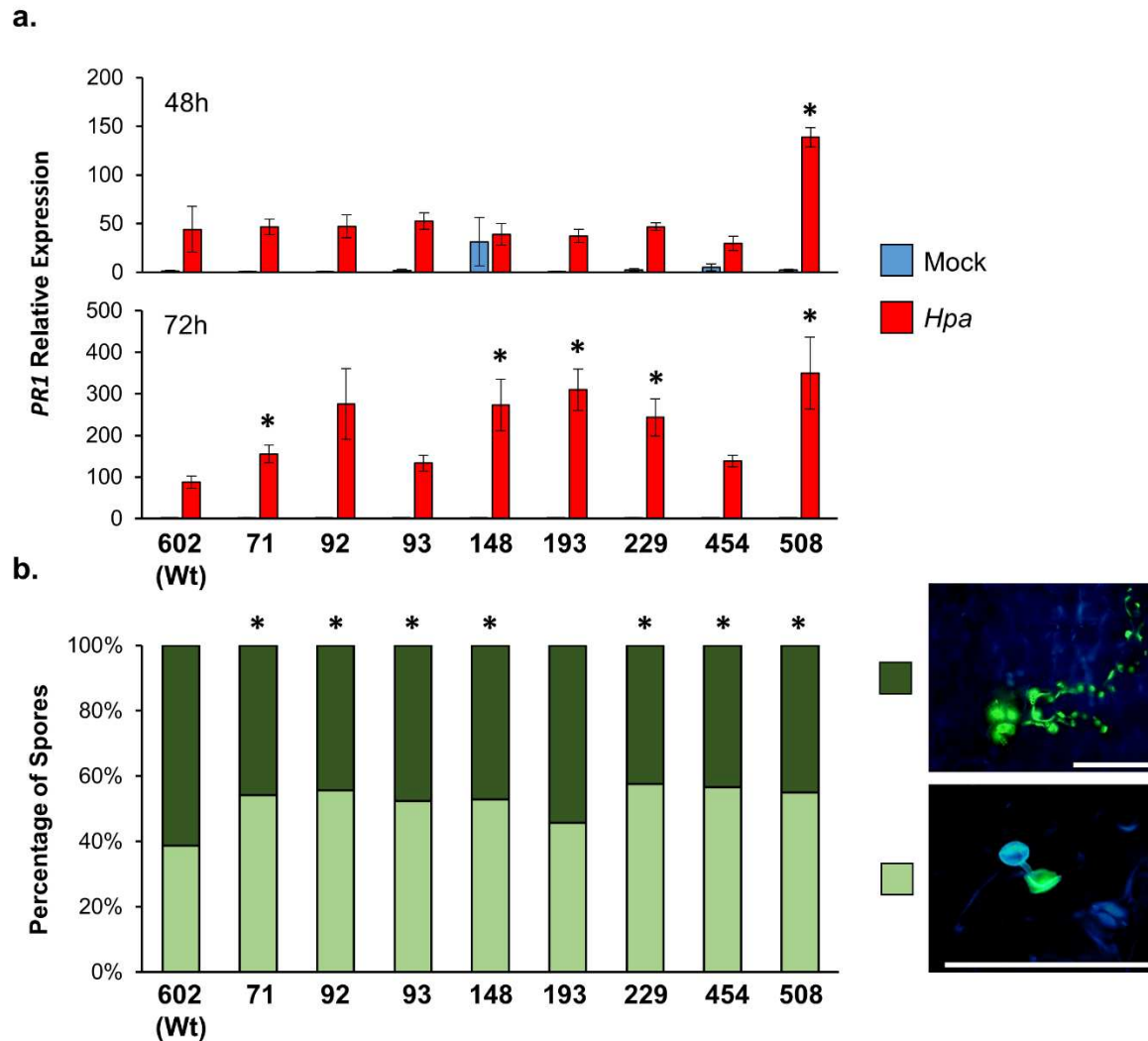


Figure 1-figure supplement 2. Average green leaf area (GLA) of the 123 epiRILs (light green), the *ddm1-2* line (F4; red) and six Wt lines (Col-0; dark green). Shown are average GLA values of three-week-old plants (\pm SEM).



752

753 **Figure 1-figure supplement 3. Resistance phenotypes of the 8 most Hpa-resistant epiRILs against different**
754 **(a) biotic stresses. a:** Confirmation of resistance against biotrophic Hpa. Shown are levels of infection at six days
755 post inoculation (dpi) of three-week-old plants. Trypan blue-stained leaves were analysed by microscopy and
756 assigned to 4 Hpa infection classes (insets on the right; see Figure 1-figure supplement 1 for further details).
757 Statistically significant differences in class distribution (asterisks) were analysed using Pearson's Chi-squared
758 tests ($p < 0.05$) in pairwise comparisons with Wt line (#602); $n > 80$. **b:** Quantification of resistance against
759 necrotrophic *Plectosphaerella cucumerina* (Pc). Shown are average lesion diameters (\pm SEM) at nine days after
760 droplet inoculation with Pc spores onto similarly aged leaves of five-week-old plants. Insets show representative
761 examples of necrotic lesions by Pc. Statistically significant differences in necrotic lesions diameter (asterisks)
762 were quantified by two-tailed Student's t-test ($p < 0.05$) in pairwise comparisons with Wt line (#602); $n = 40-48$. **c.**
763 Quantification of salt (NaCl) tolerance. Shown are percentages of seedlings developing full cotyledons after six
764 days of growth on agar with increasing NaCl concentrations. Statistically significant differences in germination
765 rates (asterisks) were quantified by Fisher's exact test ($p < 0.05$) in pairwise comparisons with Wt line (#602) at
766 each salt concentration; $n > 50$.



767

768

769

770

771

772

773

774

775

776

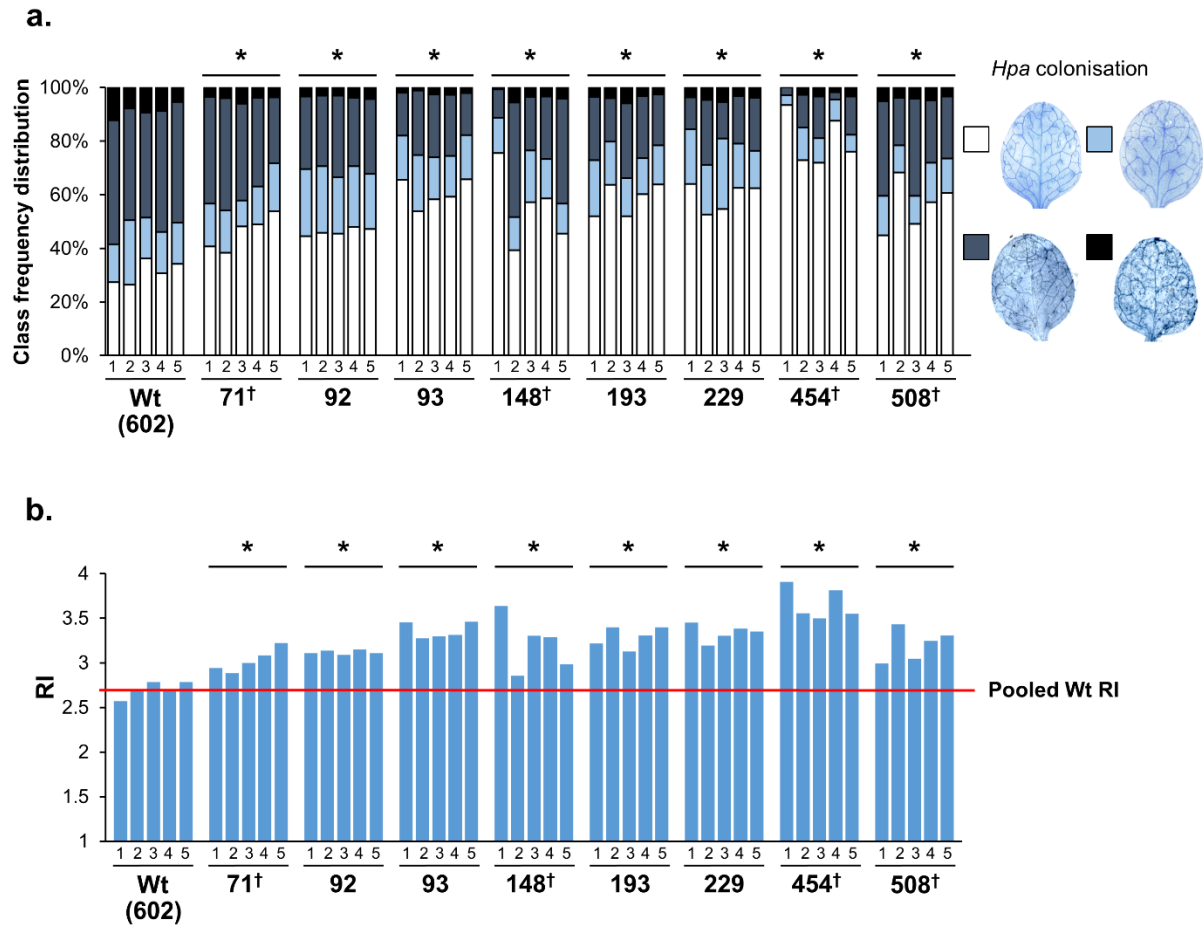


Figure 1-figure supplement 5. Transgenerational stability of Hpa resistance in Hpa-resistant epiRILs.

Five individual F9 plants from the 8 most resistant epiRILs and the Wt line (#602) were self-pollinated to generate 40 F10 families. Plants of each F10 family were analysed for Hpa colonisation at 6 dpi. **a:** Shown are frequency distributions of leaves across 4 Hpa colonisation classes (insets on the right; see Figure 1-figure supplement 1 for further details). **b:** Resistance index (RI) values of the F10 families. The red line indicates the average RI value of the Wt (#602). Asterisks at the top of each graph indicate statistically significant differences in class distribution between pooled F10 families of the epiRIL relative to pooled F10 families of the Wt line (Pearson's Chi-squared test; $p < 0.05$). Crosses (†) at the bottom of each graph indicate statistically significant differences between F10 families within each epiRIL (Pearson's Chi-squared test; $p < 0.05$).

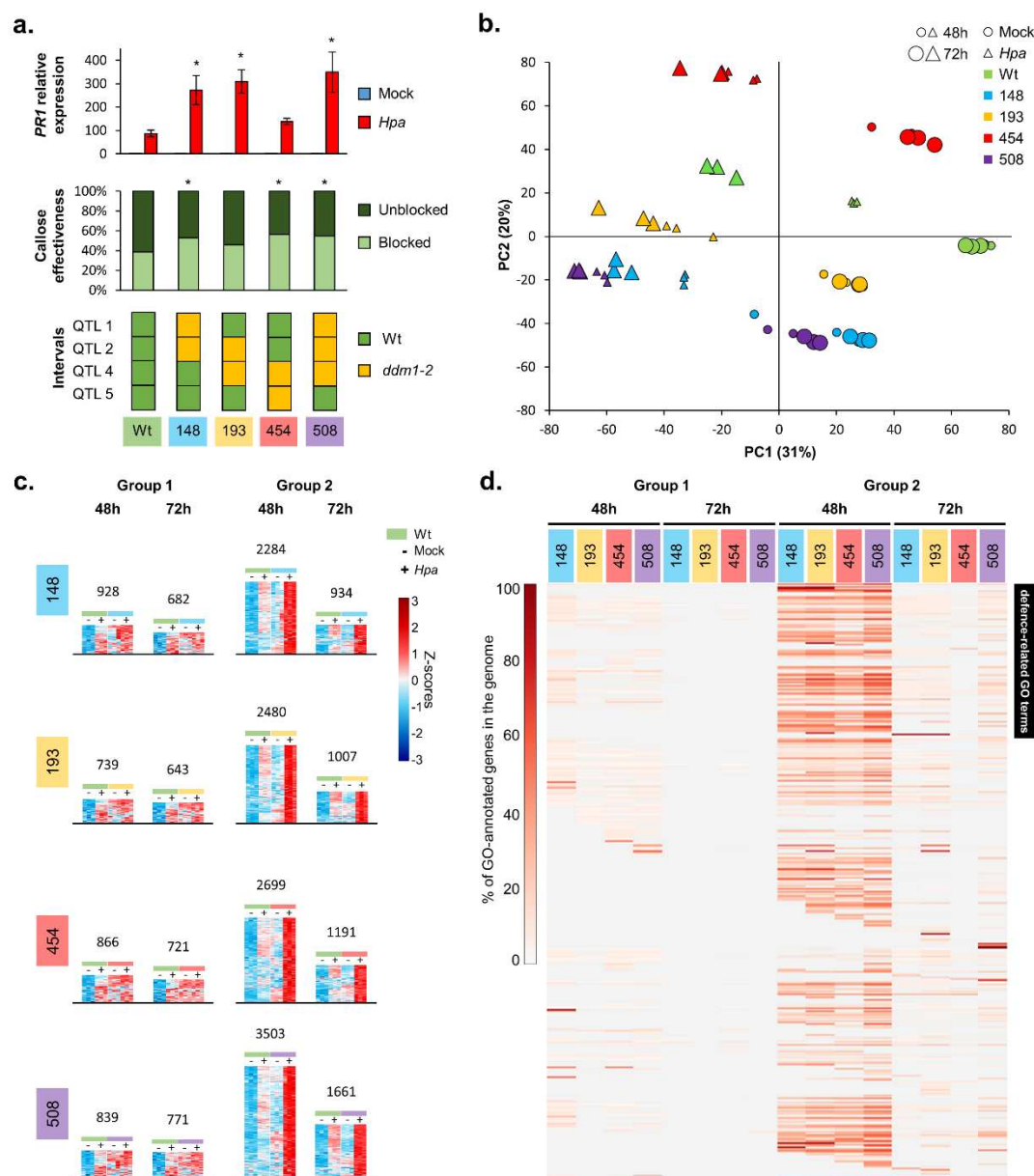


Figure 2. The defence-related transcriptome of Hpa-resistant epiRILs. **a:** Defence marker phenotypes and epiQTL haplotypes of 4 Hpa-resistant epiRILs and the Wt (#602), which were analysed by RNA sequencing. Top graph: relative expression of SA-dependent PR1 at 72 hours after inoculation (hpi) with Hpa (red) or water (blue). Middle graph: resistance efficiency of callose deposition in Hpa-inoculated plants. Shown are percentages of arrested (light) and non-arrested (dark) germ tubes at 48 hpi. Bottom panel: epiQTL haplotypes of selected lines. Green: methylated Wt haplotype; yellow: hypomethylated ddm1-2 haplotype. Asterisks indicate statistically significant differences to the Wt. (see Figure 1-figure supplement 4 for statistical information). **b:** Principal component analysis of 27,641 genes at 48 (small symbols) and 72 (large symbols) hpi with Hpa (triangles) or water (Mock; circles). Colours indicate different lines. **c:** Numbers and expression profiles of Hpa-inducible genes that show constitutively enhanced expression (Group 1) or augmented levels of Hpa-induced expression (Group 2) in the Hpa-resistant epiRILs at 48 or 72 hpi. Heatmaps show normalised standard deviations from the mean (z-scores) for each gene (rows), using rlog-transformed read counts (see Figure 2-figure supplements 3 and 4 for better detail). **d:** GO term enrichment of primed and constitutively up-regulated genes. Shown are 469 GO terms (rows), for which one or more epiRIL(s) displayed a statistically significant enrichment in one or more categories (Hypergeometric test, followed by Benjamini-Hochberg FDR correction; $q < 0.05$). Heatmap-projected values for each GO term (rows) represent percentage of GO-annotated genes in each category relative to all GO-annotated genes in the Arabidopsis genome (TAIR10). Black bar on the top right indicates 111 defence-related GO terms.

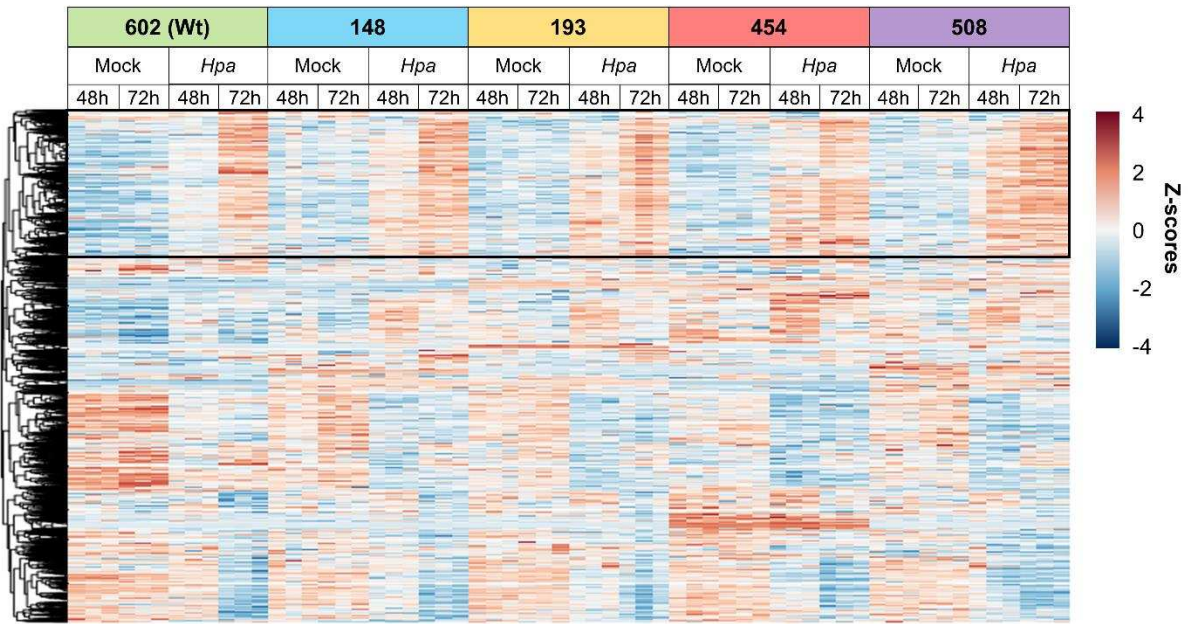
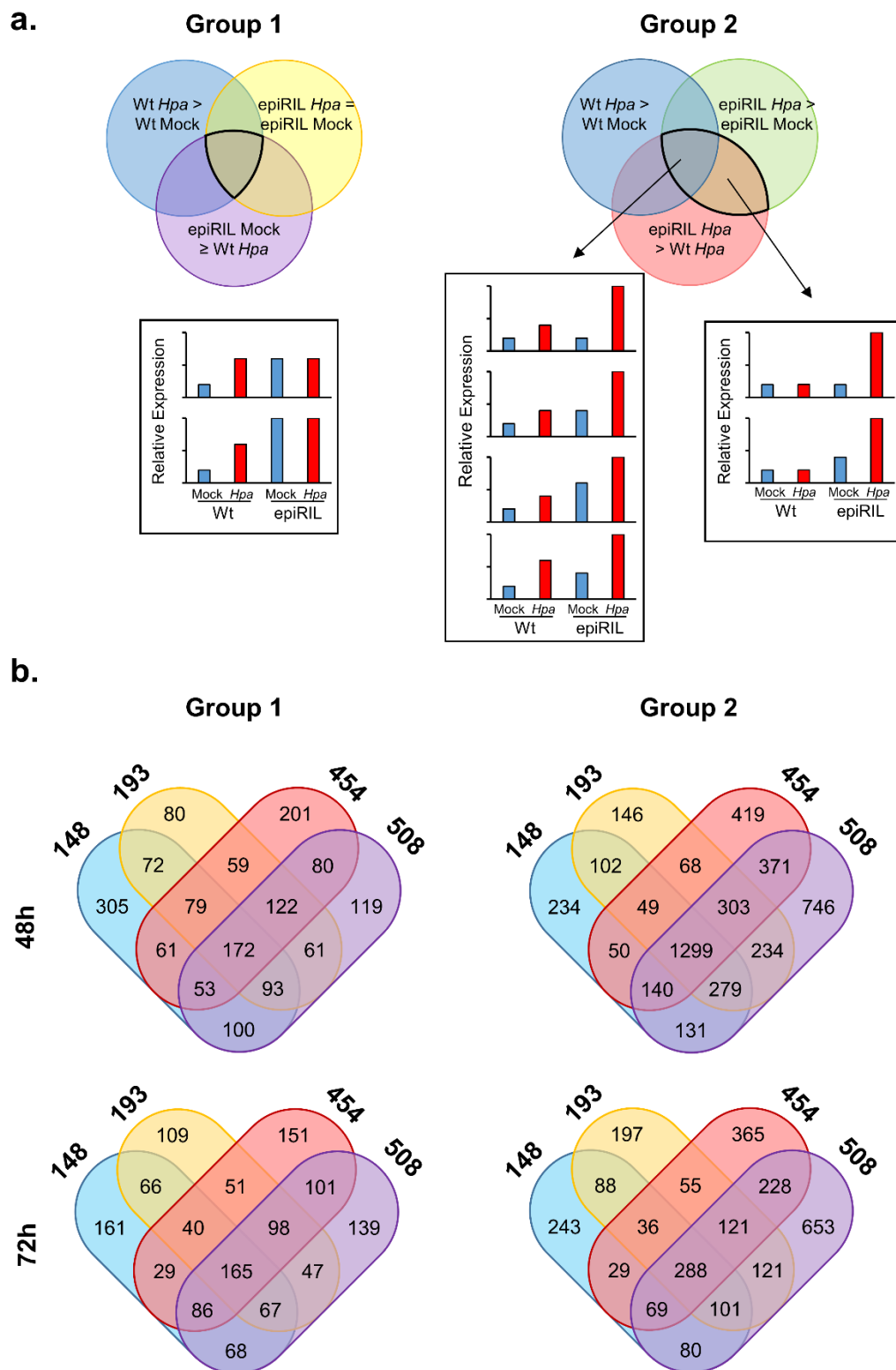


Figure 2-figure supplement 1. Hierarchical clustering of differentially expressed genes (DEGs) in selected Hpa-resistant epiRILs and the Wt at 48 and 72 hpi (Ward method). The heatmap shows normalised standard deviations from the mean (z-scores) for each DEG (rows), using rlog-transformed read counts. Columns represent three biological replicates for each line-treatment-timepoint combination. The black square at the top of the heatmap indicates a cluster with genes that show augmented induction in one or more resistant epiRILs at 48 h after Hpa inoculation.



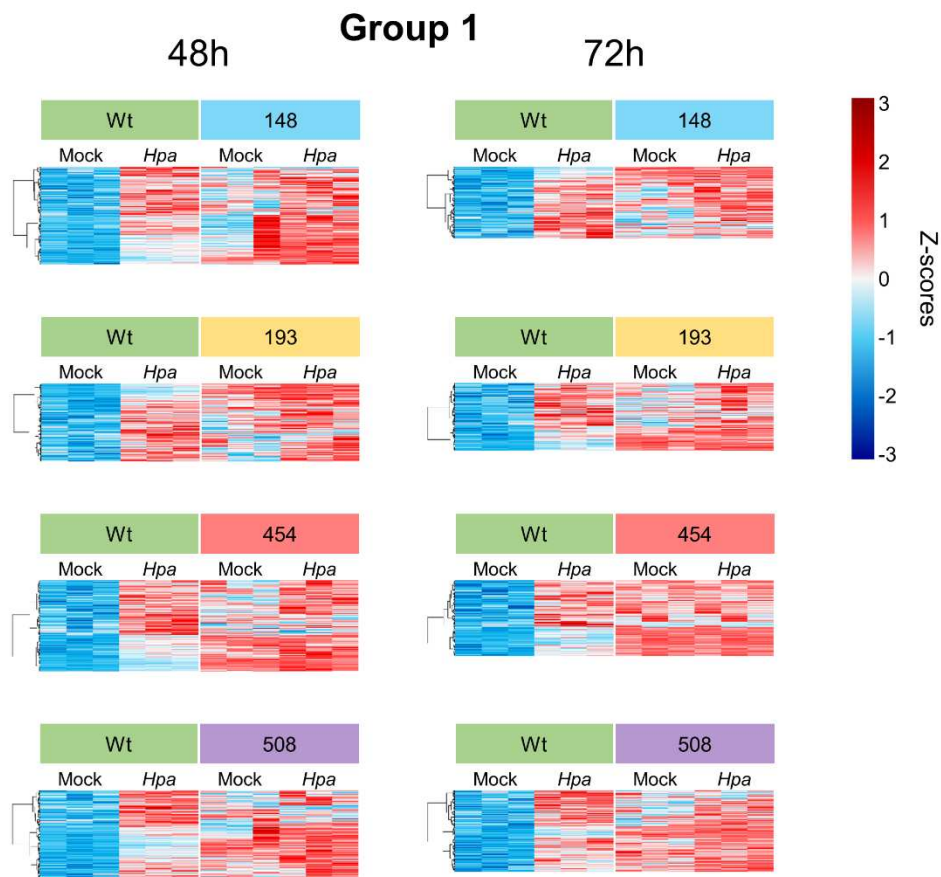
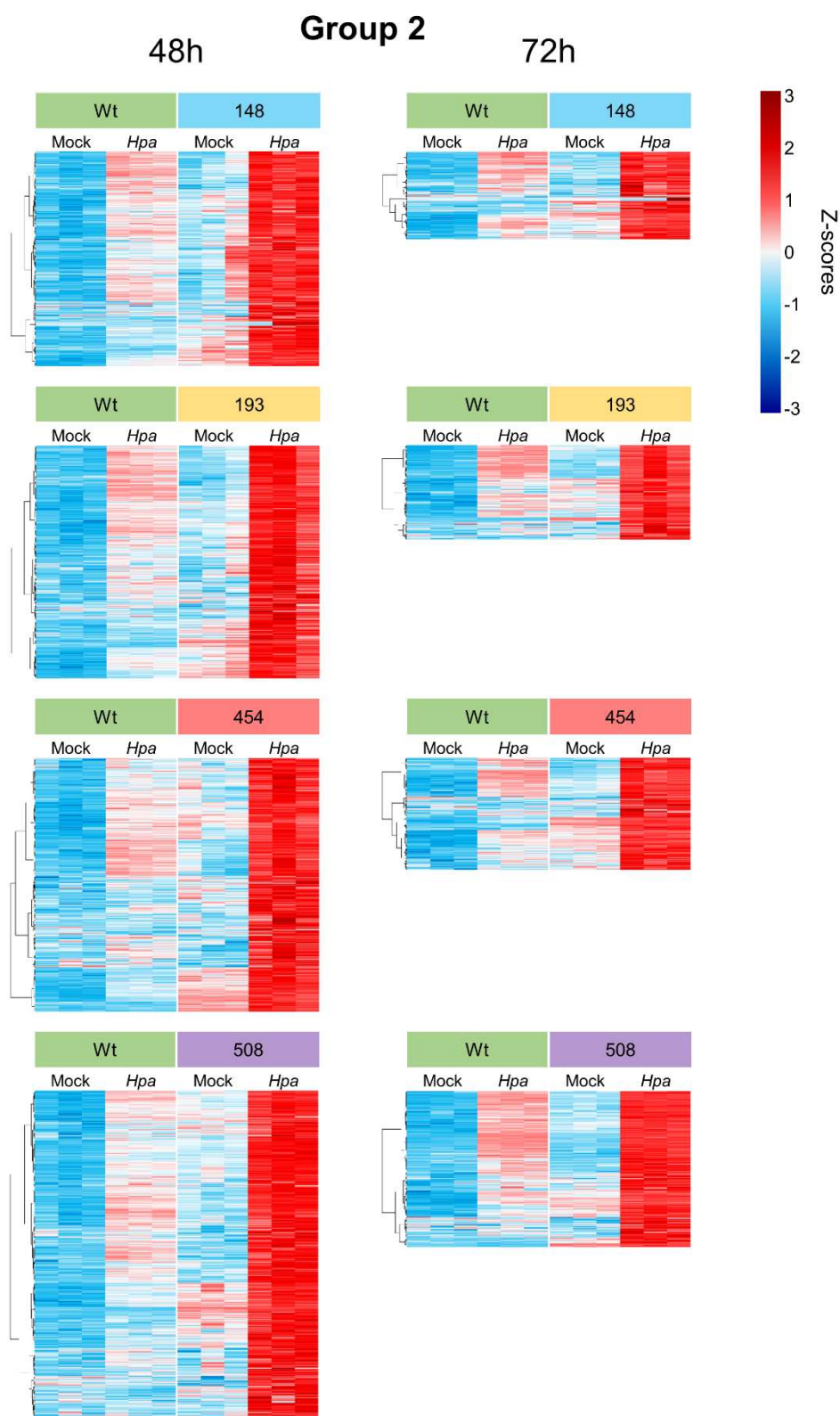


Figure 2-figure supplement 3. Transcript profiles of Hpa-inducible genes showing constitutively enhanced expression in the Hpa-resistant epiRILs (Group 1). Heatmaps show normalised standard deviations from the mean (z-scores) for each gene (rows) at 48 and 72 hpi, using rlog-transformed read counts. Columns represent three biological replicates for each line-treatment combination. Expression profiles were subjected to hierarchical clustering by gene (Ward method).



827 .

828 **Figure 2-figure supplement 4. Transcript profiles of Hpa-inducible genes showing enhanced levels of Hpa-**
 829 **induced expression in the Hpa-resistant epiRILs (Group 2).** Heatmaps show normalised standard deviations
 830 from the mean (z-scores) for each gene (rows) at 48 and 72 hpi, using rlog-transformed read counts. Columns
 831 represent three biological replicates for each line-treatment combination. Expression profiles were subjected to
 832 hierarchical clustering by gene (Ward method).

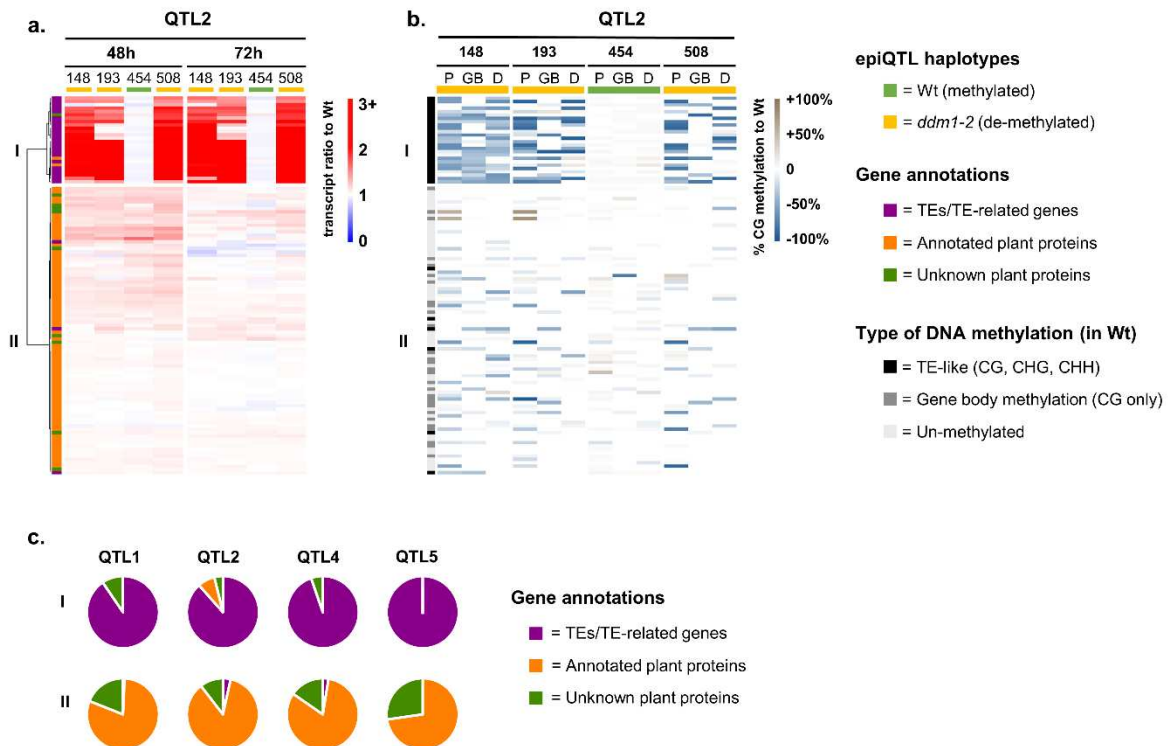


Figure 3. Relationship between augmentation of pathogen-induced expression and DNA methylation for epiQTL-localised genes. **a:** Expression profiles of epiQTL-based genes showing elevated levels of Hpa-induced expression in one or more epiRIL(s) (Group 2). Shown are genes located in the epiQTL interval of chromosome II (epiQTL2; LOD drop-off = 2; see Figure 3-figure supplement 1a for other the epiQTLs). Heatmap shows gene expression ratios between Hpa-inoculated epiRILs and the Wt, representing augmented expression levels during pathogen attack. Hierarchical clustering yielded two distinctly regulated gene clusters (I and II). Coloured bars on the top indicate epiQTL2 haplotypes. Green: methylated Wt haplotype. Yellow: hypomethylated *ddm1-2* haplotype. **b:** Levels of CG DNA methylation of the same genes in the epiQTL2 interval (see Figure 3-figure supplement 1b for other epiQTLs). Heatmap shows percentages of hypomethylation (blue) or hyper-methylation (brown) relative to the Wt for 2kb promoter regions (P), gene bodies (GB) and 1kb downstream regions (D). **c:** Distribution of gene annotations of distinctly regulated gene clusters for each epiQTL.

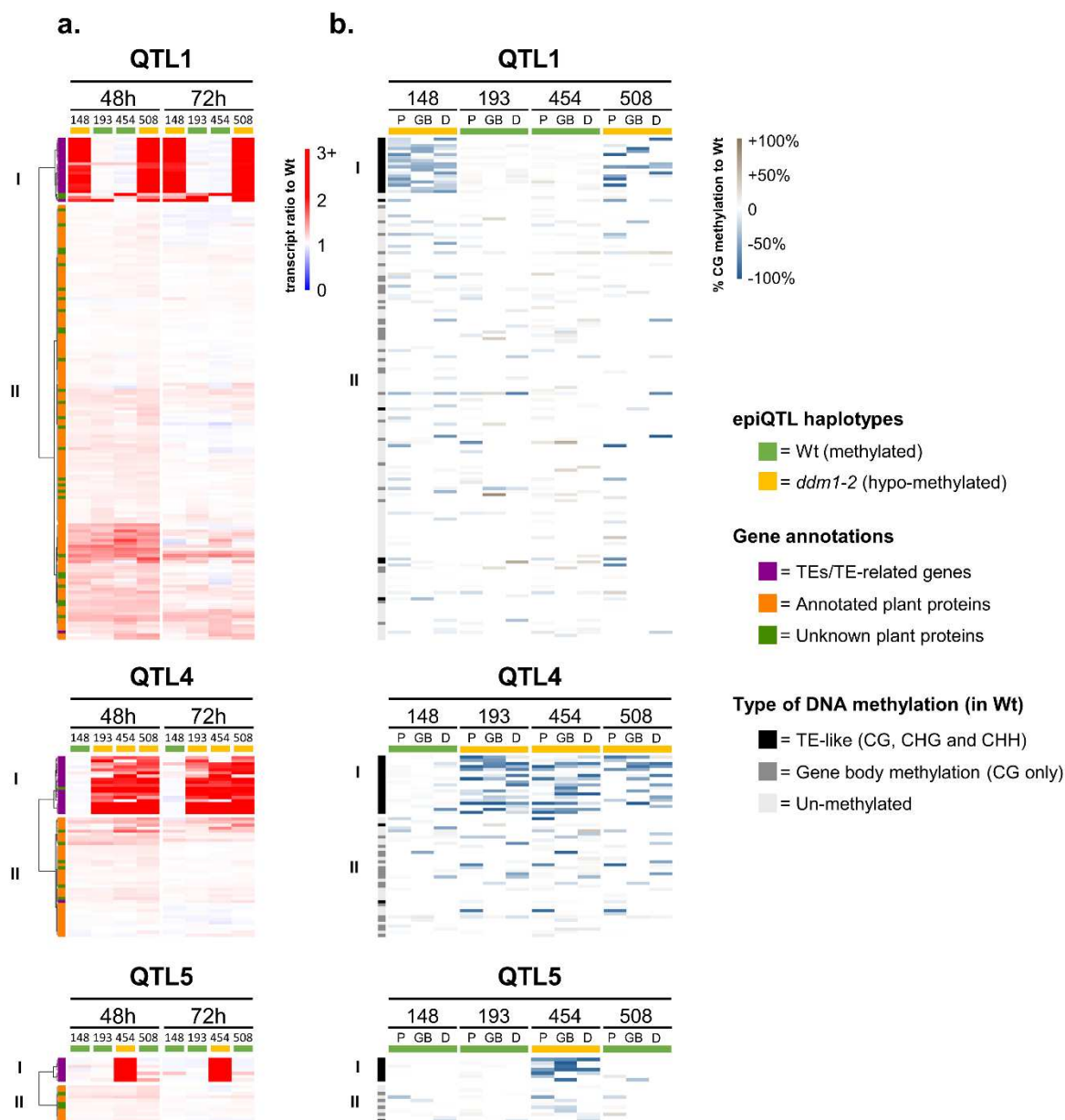


Figure 3-figure supplement 1. Relationship between augmentation of pathogen-induced expression and DNA methylation for epiQTL-localised genes. **a:** Expression profiles of epiQTL-based genes with elevated levels of Hpa-induced expression in one or more epiRILs (Group 2). Shown are genes located in the epiQTL intervals (LOD drop-off = 2) of chromosomes I (epiQTL1), chromosome IV (epiQTL4) and chromosome V (epiQTL5). **b:** Levels of DNA methylation of the same genes in epiQTL1, epiQTL4 and epiQTL5. For details, see legend to Figure 3.

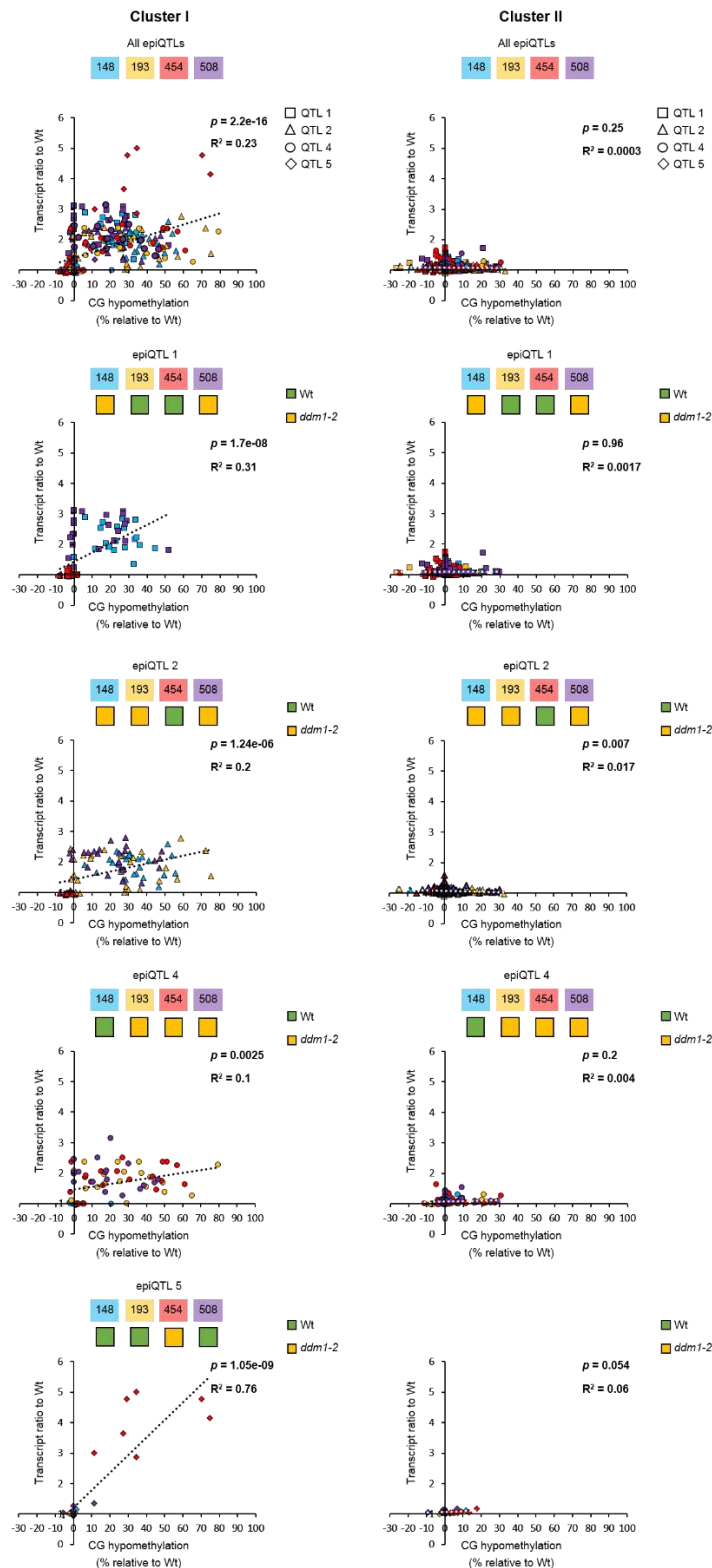


Figure 3-figure supplement 2. Correlation analysis between augmented gene transcription and DNA hypomethylation. Augmented gene transcription was defined as the ratio between the Hpa-inoculated epiRIL and the Hpa-inoculated Wt at 48 hpi (Figure 3a and Figure 3-figure supplement 1a). DNA hypomethylation values were averaged across promoter regions, gene bodies and downstream regions. Scatter plots show transcript ratios against the hypomethylation for each gene in expression clusters I and II of Group 2 (Figure 3b and Figure 3-figure supplement 1b), which were selected by hierarchical clustering of augmented expression profiles in the epiRILs during Hpa infection. Significant positive correlations (Pearson linear regression; $p < 0.05$) indicate cis-regulation by DNA methylation.

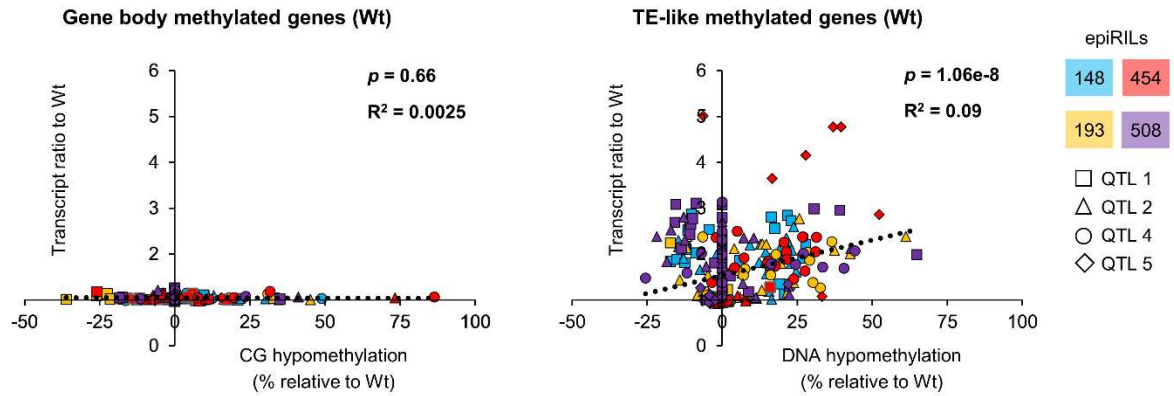


Figure 3-figure supplement 3. Correlation analysis between augmented gene transcription and type of DNA hypomethylation. Scatter plots show augmented transcript ratios against hypomethylation for all epiQTL-based genes in Group 2 (Figure 3 and Figure 3-figure supplement 1). Augmented transcription was defined as the ratio between the Hpa-inoculated epiRIL and the Hpa-inoculated Wt at 48 hpi (Figure 3a and Figure 3-figure supplement 1a). Hypomethylation values at gene bodies in the epiRILs were divided according to the type DNA methylation. If hypomethylation occurred at CG context only, genes were classified as being reduced in gene body methylation (gbM); if hypomethylation occurred all three sequence contexts (CG, CHG, CHH), genes were classified as being reduced in TE methylation (teM). Values of gbM hypomethylation are expressed as percentage reduction in GC methylation relative to the Wt; values of teM hypomethylation are expressed as percentage reduction in all sequence contexts. Statistically significant correlations (Pearson linear regression; $p < 0.05$) indicate cis-regulation by DNA methylation.

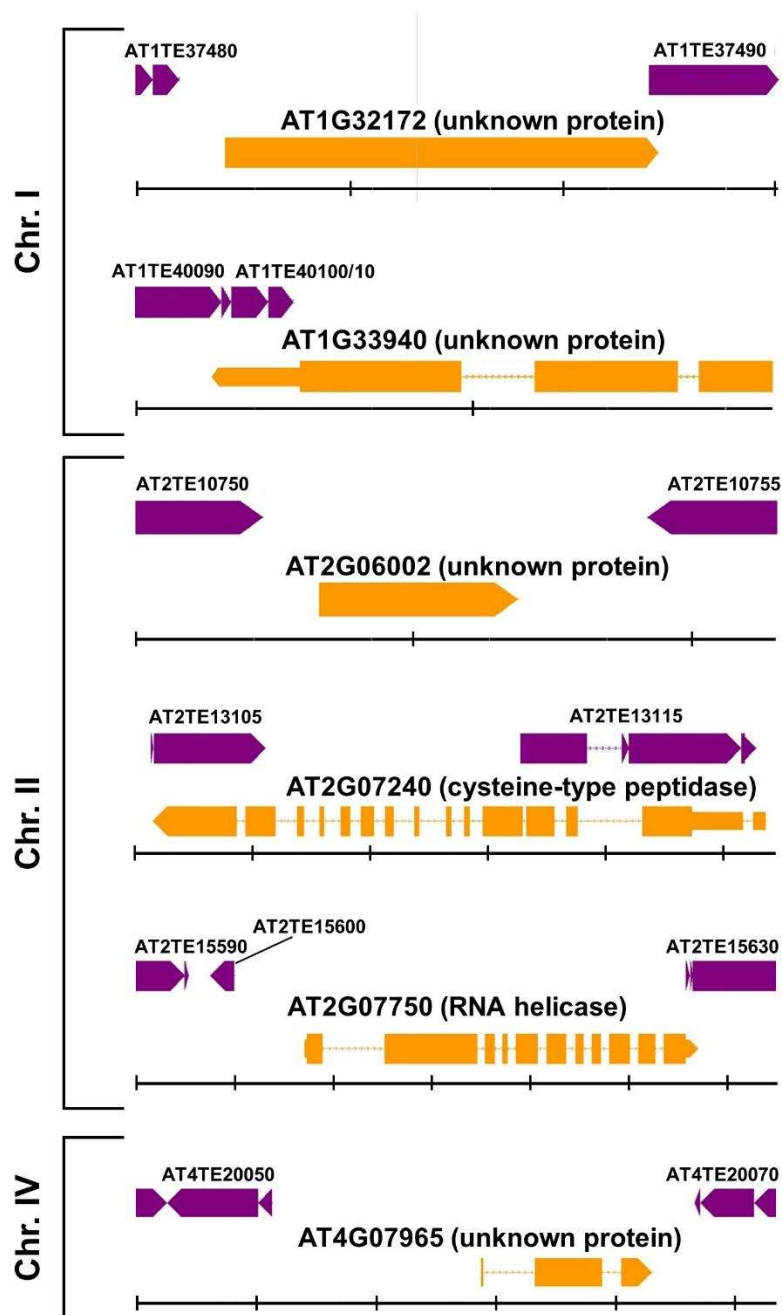


Figure 3-figure supplement 4. Genomic contexts of six plant protein-encoding genes in the epiQTL intervals, whose transcriptional priming coincides with reduced DNA methylation. Orange bars indicate gene models; superimposed purple bars indicate associated transposable elements (TEs). Large blocks represent exons; lines between blocks represent introns; smaller blocks at the 3' and 5' ends represent un-translated regions. Units of the back scale correspond to 1Kb.

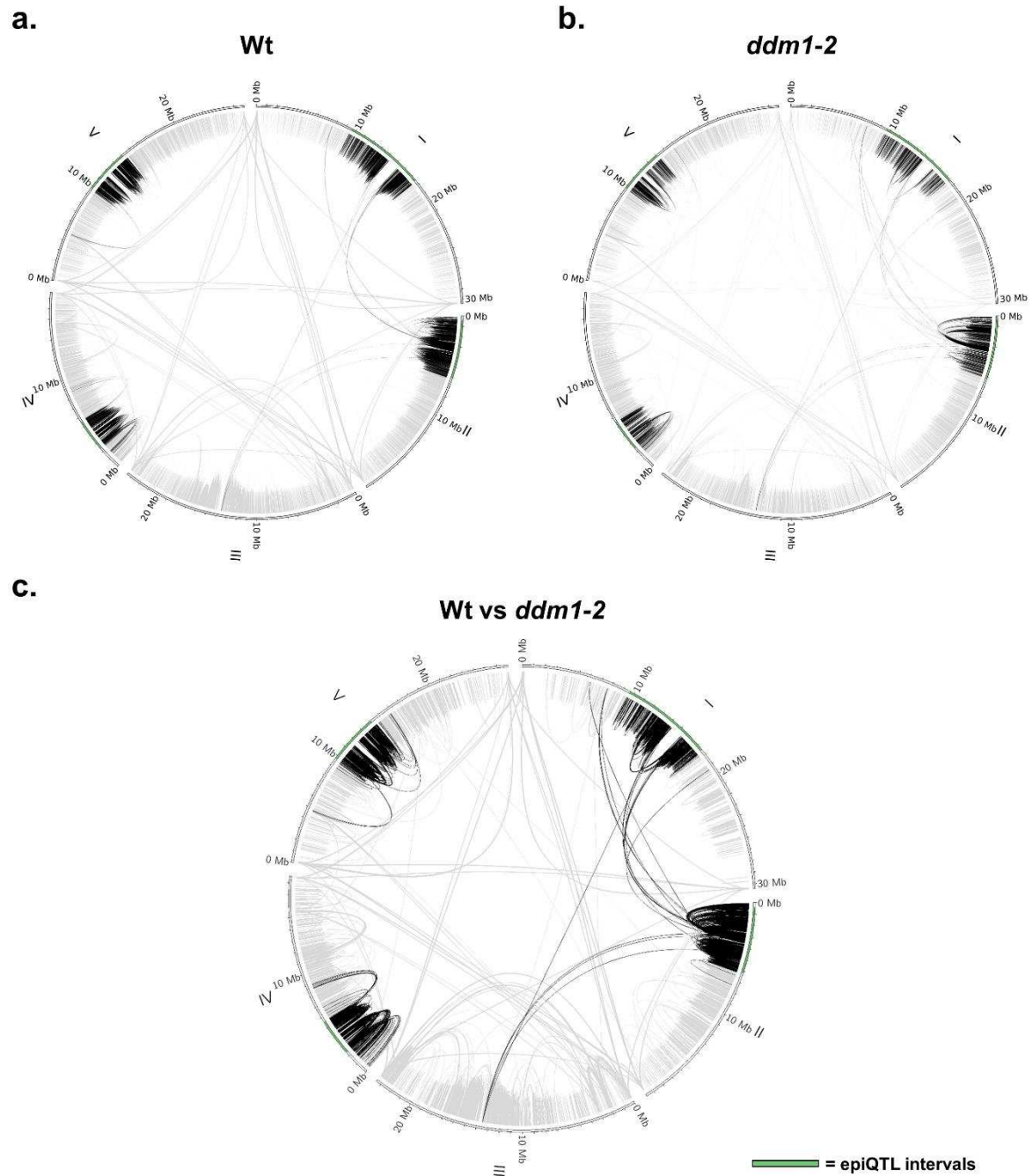


Figure 3-figure supplement 5. Genome-wide chromatin interactions in Wt and *ddm1-2* Arabidopsis. Circular diagrams show all five Arabidopsis chromosomes. The 4 epiQTL regions are highlighted in green. Chromatin interactions are indicated by lines. Gray lines: interactions outside the epiQTLs. Black lines: interactions with the epiQTLs. Presented results are based on Hi-C data from Feng et al. (2014)⁶² **a.** Genome-wide chromatin interactions in the Wt (Col-0). **b.** Genome-wide chromatin interactions in the *ddm1-2* mutant. **c.** DDM1-dependent chromatin interactions that are altered in the *ddm1-2* mutant compared to the Wt plants.

References

- 1 Vanyushin, B. F. in *DNA Methylation: Basic Mechanisms* (eds Walter Doerfler & Petra Böhm) 67-122 (Springer Berlin Heidelberg, 2006).
- 2 Law, J. A. & Jacobsen, S. E. Establishing, maintaining and modifying DNA methylation patterns in plants and animals. *Nat Rev Genet.* **11**, (2010).
- 3 Quadrana, L. & Colot, V. Plant Transgenerational Epigenetics. *Annual review of genetics* **50**, 467-491, (2016).
- 4 Espinas, N. A., Saze, H. & Saijo, Y. Epigenetic control of defense signaling and priming in plants. *Front Plant Sci* **7**, (2016).
- 5 Conrath, U. et al. Priming: Getting Ready for Battle. *Molecular Plant-Microbe Interactions* **19**, 1062-1071, (2006).
- 6 Conrath, U., Beckers, G. J. M., Langenbach, C. J. G. & Jaskiewicz, M. R. Priming for Enhanced Defense. *Annual Review of Phytopathology* **53**, 97-119, (2015).
- 7 Martinez-Medina, A. et al. Recognizing Plant Defense Priming. *Trends in Plant Science* **21**, 818-822, (2016).
- 8 Liégard, B. et al. Quantitative resistance to clubroot infection mediated by transgenerational epigenetic variation in Arabidopsis. *New Phytologist* **0**.
- 9 Jaskiewicz, M., Conrath, U. & Peterhänsel, C. Chromatin modification acts as a memory for systemic acquired resistance in the plant stress response. *EMBO reports* **12**, 50-55, (2011).
- 10 Luna, E., Bruce, T. J. A., Roberts, M. R., Flors, V. & Ton, J. Next-Generation Systemic Acquired Resistance. *Plant Physiology* **158**, 844-853, (2012).
- 11 Slaughter, A. et al. Descendants of Primed Arabidopsis Plants Exhibit Resistance to Biotic Stress. *Plant Physiology* **158**, 835-843, (2012).
- 12 Lopez, A., Ramirez, V., Garcia-Andrade, J., Flors, V. & Vera, P. in *PLoS genetics* Vol. 7 e1002434 (2011).
- 13 Luna, E. & Ton, J. The epigenetic machinery controlling transgenerational systemic acquired resistance. *Plant Signal Behav* **7**, (2012).
- 14 López Sánchez, A., Stassen, J. H. M., Furci, L., Smith, L. M. & Ton, J. The role of DNA (de)methylation in immune responsiveness of Arabidopsis. *The Plant Journal* **88**, 361-374, (2016).
- 15 Yu, A. et al. Dynamics and biological relevance of DNA demethylation in Arabidopsis antibacterial defense. *Proceedings of the National Academy of Sciences* **110**, 2389-2394, (2013).
- 16 Reinders, J. et al. Compromised stability of DNA methylation and transposon immobilization in mosaic Arabidopsis epigenomes. *Genes & development* **23**, 939-950, (2009).
- 17 Johannes, F. et al. Assessing the impact of transgenerational epigenetic variation on complex traits. *PLoS genetics* **5**, (2009).
- 18 Jeddeloh, J. A., Bender, J. & Richards, E. J. The DNA methylation locus DDM1 is required for maintenance of gene silencing in Arabidopsis. *Genes & development* **12**, 1714-1725, (1998).
- 19 Brzeski, J. & Jerzmanowski, A. Deficient in DNA Methylation 1 (DDM1) Defines a Novel Family of Chromatin-remodeling Factors. *The Journal of biological chemistry* **278**, (2003).
- 20 Zemach, A. et al. The Arabidopsis Nucleosome Remodeler DDM1 Allows DNA Methyltransferases to Access H1-Containing Heterochromatin. *Cell* **153**, 193-205, (2013).
- 21 Kakutani, T., Jeddeloh, J. A., Flowers, S. K., Munakata, K. & Richards, E. J. Developmental abnormalities and epimutations associated with DNA hypomethylation mutations. *Proceedings of the National Academy of Sciences of the United States of America* **93**, (1996).
- 22 Ito, T. et al. Genome-Wide Negative Feedback Drives Transgenerational DNA Methylation Dynamics in Arabidopsis. *PLoS genetics* **11**, e1005154, (2015).
- 23 Colomé-Tatché, M. et al. Features of the Arabidopsis recombination landscape resulting from the combined loss of sequence variation and DNA methylation. *Proceedings of the National Academy of Sciences* **109**, 16240-16245, (2012).
- 24 Latzel, V. et al. Epigenetic diversity increases the productivity and stability of plant populations. *Nature Communications* **4**, 2875, (2013).

954 25 Cortijo, S. et al. Mapping the Epigenetic Basis of Complex Traits. *Science* **343**, 1145-1148,
955 (2014).

956 26 Kooke, R. et al. Epigenetic Basis of Morphological Variation and Phenotypic Plasticity in
957 *Arabidopsis thaliana*. *The Plant Cell Online* **27**, 337-348, (2015).

958 27 Matzke, M. A. & Mosher, R. A. RNA-directed DNA methylation: an epigenetic pathway of
959 increasing complexity. *Nat Rev Genet.* **15**, (2014).

960 28 Gilly, A. et al. TE-Tracker: systematic identification of transposition events through whole-
961 genome resequencing. *BMC Bioinformatics* **15**, 1-16, (2014).

962 29 Huot, B., Yao, J., Montgomery, B. L. & He, S. Y. Growth–Defense Tradeoffs in Plants: A
963 Balancing Act to Optimize Fitness. *Molecular Plant* **7**, 1267-1287, (2014).

964 30 Koornneef, A. & Pieterse, C. M. J. Cross Talk in Defense Signaling. *Plant Physiology* **146**,
965 839-844, (2008).

966 31 Knoth, C., Ringler, J., Dangl, J. L. & Eulgem, T. *Arabidopsis* WRKY70 Is Required for Full
967 RPP4-Mediated Disease Resistance and Basal Defense Against *Hyaloperonospora parasitica*.
968 *Molecular Plant-Microbe Interactions* **20**, 120-128, (2007).

969 32 Coates, M. E. & Beynon, J. *Hyaloperonospora arabidopsidis* as a Pathogen Model. *Annual*
970 *Review of Phytopathology* **48**, 329-345, (2010).

971 33 Koch, E. & Slusarenko, A. *Arabidopsis* is susceptible to infection by a downy mildew fungus.
972 *The Plant cell* **2**, 437-445, (1990).

973 34 Soylu, E. M. & Soylu, S. Light and Electron Microscopy of the Compatible Interaction Between
974 *Arabidopsis* and the Downy Mildew Pathogen *Peronospora parasitica*. *Journal of*
975 *Phytopathology* **151**, 300-306, (2003).

976 35 Luna, E. et al. Callose Deposition: A Multifaceted Plant Defense Response. *Molecular Plant-*
977 *Microbe Interactions* **24**, 183-193, (2010).

978 36 Jantzen, S. G., Sutherland, B. J., Minkley, D. R. & Koop, B. F. GO Trimming: Systematically
979 reducing redundancy in large Gene Ontology datasets. *BMC Research Notes* **4**, 267, (2011).

980 37 Bewick, A. J. et al. The evolution of CHROMOMETHYLASES and gene body DNA
981 methylation in plants. *Genome biology* **18**, 65, (2017).

982 38 Schmitz, R. J. et al. Patterns of population epigenomic diversity. *Nature* **495**, (2013).

983 39 Roux, F. et al. Genome-wide epigenetic perturbation jump-starts patterns of heritable variation
984 found in nature. *Genetics* **188**, (2011).

985 40 Mauch-Mani, B., Baccelli, I., Luna, E. & Flors, V. Defense Priming: An Adaptive Part of
986 Induced Resistance. *Annual Review of Plant Biology* **68**, 485-512, (2017).

987 41 Wibowo, A. et al. Hyperosmotic stress memory in *Arabidopsis* is mediated by distinct
988 epigenetically labile sites in the genome and is restricted in the male germline by DNA
989 glycosylase activity. *eLife* **5**, e13546, (2016).

990 42 Rasmann, S. et al. Herbivory in the Previous Generation Primes Plants for Enhanced Insect
991 Resistance. *Plant Physiology* **158**, 854-863, (2012).

992 43 Aller, E. S. T., Jagd, L. M., Kliebenstein, D. J. & Burow, M. Comparison of the Relative
993 Potential for Epigenetic and Genetic Variation To Contribute to Trait Stability. *G3:*
994 *Genes|Genomes|Genetics* **8**, 1733-1746, (2018).

995 44 Ishida, M., Hara, M., Fukino, N., Kakizaki, T. & Morimitsu, Y. Glucosinolate metabolism,
996 functionality and breeding for the improvement of Brassicaceae vegetables. *Breeding science*
997 **64**, 48-59, (2014).

998 45 Clay, N. K., Adio, A. M., Denoux, C., Jander, G. & Ausubel, F. M. Glucosinolate Metabolites
999 Required for an *Arabidopsis* Innate Immune Response. *Science* **323**, 95-101, (2009).

1000 46 Bednarek, P. et al. A Glucosinolate Metabolism Pathway in Living Plant Cells Mediates Broad-
1001 Spectrum Antifungal Defense. *Science* **323**, 101-106, (2009).

1002 47 van Hulten, M., Pelser, M., van Loon, L. C., Pieterse, C. M. J. & Ton, J. Costs and benefits of
1003 priming for defense in *Arabidopsis*. *Proceedings of the National Academy of Sciences* **103**,
1004 5602-5607, (2006).

1005 48 Soppe, W. J. J. et al. The late flowering phenotype of *fwa* mutants is caused by gain-of-function
1006 epigenetic alleles of a homeodomain gene. *Molecular cell* **6**, (2000).

1007 49 Saze, H. & Kakutani, T. Heritable epigenetic mutation of a transposon-flanked Arabidopsis
 1008 gene due to lack of the chromatin-remodeling factor DDM1. *The EMBO journal* **26**, 3641-3652,
 1009 (2007).
 1010 50 Kinoshita, Y. et al. Control of FWA gene silencing in Arabidopsis thaliana by SINE-related
 1011 direct repeats. *The Plant Journal* **49**, 38-45, (2007).
 1012 51 Lei, M. et al. Regulatory link between DNA methylation and active demethylation in
 1013 Arabidopsis. *Proceedings of the National Academy of Sciences of the United States of America*
 1014 **112**, (2015).
 1015 52 Williams, B. P., Pignatta, D., Henikoff, S. & Gehring, M. Methylation-sensitive expression of
 1016 a DNA demethylase gene serves as an epigenetic rheostat. *PLoS genetics* **11**, (2015).
 1017 53 Panda, K. et al. Full-length autonomous transposable elements are preferentially targeted by
 1018 expression-dependent forms of RNA-directed DNA methylation. *Genome biology* **17**, 170,
 1019 (2016).
 1020 54 Cambiagno, D. A. et al. Immune receptor genes and pericentromeric transposons as targets of
 1021 common epigenetic regulatory elements. *The Plant Journal*, (2018).
 1022 55 Liu, C. et al. Arabidopsis ARGONAUTE 1 Binds Chromatin to Promote Gene Transcription
 1023 in Response to Hormones and Stresses. *Developmental Cell* **44**, 348-361.e347, (2018).
 1024 56 Wang, D. et al. Transposable elements (TEs) contribute to stress-related long intergenic
 1025 noncoding RNAs in plants. *The Plant Journal* **90**, 133-146, (2017).
 1026 57 Heo, J. B., Lee, Y.-S. & Sung, S. Epigenetic regulation by long noncoding RNAs in plants.
 1027 *Chromosome Research* **21**, 685-693, (2013).
 1028 58 Quinodoz, S. & Guttman, M. Long non-coding RNAs: An emerging link between gene
 1029 regulation and nuclear organization. *Trends in Cell Biology* **24**, 651-663, (2014).
 1030 59 Vance, K. W. & Ponting, C. P. Transcriptional regulatory functions of nuclear long noncoding
 1031 RNAs. *Trends in Genetics* **30**, 348-355, (2014).
 1032 60 Harmston, N. & Lenhard, B. Chromatin and epigenetic features of long-range gene regulation.
 1033 *Nucleic acids research* **41**, 7185-7199, (2013).
 1034 61 Liu, C. et al. Genome-wide analysis of local chromatin packing in Arabidopsis thaliana.
 1035 *Genome research* **25**, 246-256, (2016).
 1036 62 Weber, B., Zicola, J., Oka, R. & Stam, M. Plant Enhancers: A Call for Discovery. *Trends in*
 1037 *Plant Science* **21**, 974-987, (2016).
 1038 63 Wang, J. et al. Genome-Wide Analysis of the Distinct Types of Chromatin Interactions in
 1039 Arabidopsis thaliana. *Plant and Cell Physiology* **58**, 57-70, (2017).
 1040 64 Feng, S. et al. Genome-wide Hi-C Analyses in Wild-Type and Mutants Reveal High-Resolution
 1041 Chromatin Interactions in Arabidopsis. *Molecular cell* **55**, 694-707, (2014).
 1042 65 Broman, K. W., Wu, H., Sen, S. & Churchill, G. A. R/qtl: QTL mapping in experimental
 1043 crosses. *Bioinformatics* **19**, 889-890, (2003).
 1044 66 Ton, J. & Mauch-Mani, B. β -amino-butyric acid-induced resistance against necrotrophic
 1045 pathogens is based on ABA-dependent priming for callose. *The Plant Journal* **38**, 119-130,
 1046 (2004).
 1047 67 Livak, K. J. & Schmittgen, T. D. Analysis of Relative Gene Expression Data Using Real-Time
 1048 Quantitative PCR and the 2- $\Delta\Delta$ CT Method. *Methods* **25**, 402-408, (2001).
 1049 68 Czechowski, T., Stitt, M., Altmann, T., Udvardi, M. K. & Scheible, W.-R. Genome-Wide
 1050 Identification and Testing of Superior Reference Genes for Transcript Normalization in
 1051 Arabidopsis. *Plant Physiology* **139**, 5-17, (2005).
 1052 69 Andrews, S. FastQC: a quality control tool for high throughput sequence data, (2010).
 1053 70 Bolger, A. M., Lohse, M. & Usadel, B. Trimmomatic: a flexible trimmer for Illumina sequence
 1054 data. *Bioinformatics* **30**, 2114-2120, (2014).
 1055 71 Kim, D., Langmead, B. & Salzberg, S. L. HISAT: a fast spliced aligner with low memory
 1056 requirements. *Nat Meth* **12**, 357-360, (2015).
 1057 72 Anders, S., Pyl, P. T. & Huber, W. HTSeq—a Python framework to work with high-throughput
 1058 sequencing data. *Bioinformatics* **31**, 166-169, (2015).
 1059 73 Love, M. I., Huber, W. & Anders, S. Moderated estimation of fold change and dispersion for
 1060 RNA-seq data with DESeq2. *Genome biology* **15**, 550, (2014).
 1061 74 Kolde, R. "pheatmap": Pretty Heatmaps, (2015).

1062 75 Yi, X., Du, Z. & Su, Z. PlantGSEA: a gene set enrichment analysis toolkit for plant community.
1063 Nucleic acids research **41**, W98-W103, (2013).
1064 76 Lauss, K. et al. Parental DNA methylation states are associated with heterosis in epigenetic
1065 hybrids. Plant Physiology, (2017).
1066 77 Berardini, T. Z. et al. The arabidopsis information resource: Making and mining the “gold
1067 standard” annotated reference plant genome. genesis **53**, 474-485, (2015).
1068 78 Wingett, S. et al. HiCUP: pipeline for mapping and processing Hi-C data. F1000Research **4**,
1069 1310, (2015).
1070 79 Langmead, B. & Salzberg, S. L. Fast gapped-read alignment with Bowtie 2. Nature Methods **9**,
1071 357, (2012).
1072 80 Heinz, S. et al. Simple Combinations of Lineage-Determining Transcription Factors Prime cis-
1073 Regulatory Elements Required for Macrophage and B Cell Identities. Molecular cell **38**, 576-
1074 589, (2010).
1075 81 Krzywinski, M. et al. Circos: An information aesthetic for comparative genomics. Genome
1076 research **19**, 1639-1645, (2009).
1077
1078